



**GEOMETRIC APPROACH TO ORBITAL FORMATION  
MISSION DESIGN**

THESIS

Matthew J. Press, GS-11, USAF

AFIT/GA/ENY/04-M04

**DEPARTMENT OF THE AIR FORCE  
AIR UNIVERSITY**

***AIR FORCE INSTITUTE OF TECHNOLOGY***

---

**Wright-Patterson Air Force Base, Ohio**

APPROVED FOR PUBLIC RELEASE; DISTRIBUTION UNLIMITED

The views expressed in this thesis are those of the author and do not reflect the official policy or position of the United States Air Force, Department of Defense, or the United States Government.

AFIT/GA/ENY/04-M04

GEOMETRIC APPROACH TO ORBITAL FORMATION  
MISSION DESIGN

THESIS

Presented to the Faculty  
Department of Aeronautics and Astronautics  
Graduate School of Engineering and Management  
Air Force Institute of Technology  
Air University  
Air Education and Training Command  
in Partial Fulfillment of the Requirements for the  
Degree of Master of Science in Astronautical Engineering

Matthew J. Press, B.S.M.E.

GS-11, USAF

March, 2004


APPROVED FOR PUBLIC RELEASE; DISTRIBUTION UNLIMITED

GEOMETRIC APPROACH TO ORBITAL FORMATION  
MISSION DESIGN


Matthew J. Press, B.S.M.E.

GS-11, USAF

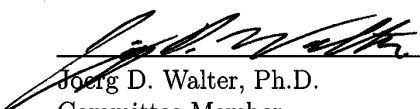
Approved:

  
\_\_\_\_\_  
Steven G. Tragesser, Ph.D.  
Thesis Advisor


11 MAR 04  
Date

  
\_\_\_\_\_  
William E. Wiesel, Ph.D.  
Committee Member

11 Mar 04  
Date

  
\_\_\_\_\_  
Joerg D. Walter, Ph.D.  
Committee Member

11 Mar 04  
Date

  
\_\_\_\_\_  
T. Alan Lovell, Ph.D.  
Committee Member

3/8/04  
Date

*Abstract*

For distributed remote sensing architectures to be useful for collecting data, it is essential to have a methodology for relating orbital formation parameters to remote sensing requirements. Utilizing the characteristics of formation parameters, an orbital design approach is developed that establishes a satellite formation from a desired instantaneous spatial distribution as viewed from a target ground site. To maintain a conceptually basic representation, a geometric approach is used to develop the correlating algorithm. This tool will enable mission planning for orbital formations as well as future concept exploration.

## *Acknowledgements*

First and foremost, I would like to thank Dr. Steven Tragesser who gave me the freedom to pursue and formulate my own ideas but whose patience and experience guided those ideas into a professional document.

In addition, I would like to acknowledge the members of my committee, Dr. Alan Lovell, Dr. Joerg Walter and Dr. William Wiesel, for their helpful insight.

This research would not have been possible without the support of Mrs. Linda Hamilton from the Human Systems Wing at Brooks City Base nor the sponsorship of Dr. Frank Chavez and Dr. Richard deJonckheere from the Space Vehicles Directorate of the Air Force Research Laboratory at Kirtland AFB, NM.

Most of all, I would like to thank my beautiful wife on whom I leaned from start to finish for her unselfish love and enduring encouragement.

Matthew J. Press

## *Table of Contents*

	Page
Abstract . . . . .	iv
Acknowledgements . . . . .	v
List of Figures . . . . .	ix
List of Symbols . . . . .	xi
 I. Introduction . . . . .	 1-1
1.1 Problem Statement . . . . .	1-1
1.2 Literature Review . . . . .	1-1
1.3 Research Objective . . . . .	1-4
1.4 Thesis Outline . . . . .	1-4
 II. Preliminary Development . . . . .	 2-1
2.1 Coordinate Systems . . . . .	2-1
2.1.1 Satellite “RSW” . . . . .	2-4
2.1.2 Relative “BAC” . . . . .	2-4
2.1.3 Earth Centered Inertial “IJK” . . . . .	2-4
2.1.4 Topocentric Horizontal “SEZ” . . . . .	2-5
2.1.5 Objectcentric Viewing “GLP” . . . . .	2-6
2.1.6 Observation “UV” . . . . .	2-6
2.2 Preliminary Equations . . . . .	2-7
2.2.1 Hill’s Equations . . . . .	2-8
2.2.2 Hill’s Stationary Solution . . . . .	2-11
 III. Stationary Formation Characteristics . . . . .	 3-1
3.1 Parameterization . . . . .	3-1
3.2 Formation Plane . . . . .	3-3
3.3 Relative Axis . . . . .	3-4
3.4 Relative Eccentricity . . . . .	3-6
3.4.1 Example . . . . .	3-6
3.5 Relative Quotient . . . . .	3-8
3.6 Formation Angles . . . . .	3-9
3.6.1 Parametric to Physical . . . . .	3-9
3.6.2 Out-of-Plane Position . . . . .	3-12

	Page
IV. Mission Design . . . . .	4-1
4.1 Preliminary Mission Design . . . . .	4-1
4.1.1 Mission Requirements . . . . .	4-1
4.1.2 Satellite Requirements . . . . .	4-1
4.1.3 Radar Requirements . . . . .	4-2
4.2 Perpendicular Constraint . . . . .	4-2
4.3 Co-formation Constraint . . . . .	4-6
4.3.1 Three Point Array (Minimizing $a_e$ ) . . . . .	4-6
4.3.2 Four Point Array . . . . .	4-10
4.4 Numerical Examples . . . . .	4-12
4.4.1 Perpendicular . . . . .	4-12
4.4.2 Minimizing $a_e$ . . . . .	4-14
4.4.3 Three Deputy Array . . . . .	4-15
V. Conclusions and Recommendations . . . . .	5-1
5.1 Conclusions . . . . .	5-1
5.2 Recommendations . . . . .	5-1
Appendix A. Trigonometric Relations . . . . .	A-1
Appendix B. MATLAB <sup>®</sup> One Axis Rotation Code . . . . .	B-1
Appendix C. MATLAB <sup>®</sup> Two Axis Rotation Code . . . . .	C-1
Appendix D. MATLAB <sup>®</sup> Three Axis Rotation Code . . . . .	D-1
Appendix E. MATLAB <sup>®</sup> GLP to SEZ . . . . .	E-1
Appendix F. MATLAB <sup>®</sup> SEZ to IJK . . . . .	F-1
Appendix G. MATLAB <sup>®</sup> IJK to RSW . . . . .	G-1
Appendix H. MATLAB <sup>®</sup> RSW to IJK . . . . .	H-1
Appendix I. MATLAB <sup>®</sup> IJK to SEZ . . . . .	I-1
Appendix J. MATLAB <sup>®</sup> SEZ to GLP . . . . .	J-1
Appendix K. MATLAB <sup>®</sup> GLP to UV . . . . .	K-1
Bibliography . . . . .	BIB-1



	Page
Vita . . . . .	VITA-1

## *List of Figures*

Figure		Page
2.1.	“BAC” Coordinate System . . . . .	2-5
2.2.	“GLP” Coordinate System . . . . .	2-7
3.1.	Physical Representation of $a_e$ , $z_{max}$ and $y_d$ . . . . .	3-2
3.2.	Physical Representation of $a_r$ and $b_r$ . . . . .	3-7
3.3.	Eccentricity Versus $q_r$ and $\phi$ in 3-D Space . . . . .	3-8
3.4.	Contour Plot of $q_r$ and $\phi$ with Constant Lines of Eccentricity	3-9
3.5.	Example: $\phi$ Versus $q_r$ When Eccentricity Equals $\frac{\sqrt{3}}{2}$ . . . . .	3-10
3.6.	$e_r$ Versus $a_e$ and $z_{max}$ for $\phi = 60^\circ$ . . . . .	3-11
3.7.	$a_e$ Versus $z_{max}$ Contour Plot for Constant $e_r$ at $\phi = 60^\circ$ . .	3-12
3.8.	Physical Representation of $\beta$ , $\tilde{\beta}$ , $\phi$ and $\tilde{\phi}$ . . . . .	3-13
3.9.	Relative Argument of Latitude . . . . .	3-14
3.10.	First-Order Force-Free Stationary Formations: In-Plane View	3-15
3.11.	First-Order Force-Free Stationary Formations: 3-D View . . .	3-16
4.1.	Two Tangent Site Vectors . . . . .	4-9
4.2.	Three Line of Sight Vectors . . . . .	4-10
4.3.	Line of Sight Vectors Intersecting a Projection Cylinder . . .	4-11
4.4.	Parallelepiped and Intersection Vectors . . . . .	4-12
4.5.	Perpendicular Constraint Example: Representation of The Reference Orbit, Target Site, and Look Vector . . . . .	4-13
4.6.	Perpendicular Constraint Example: Formation Plot with Satellites in RSW . . . . .	4-13
4.7.	Perpendicular Constraint Example: Formation Plot with Satellites in UV . . . . .	4-14
4.8.	Minimum $a_e$ Example: Representation of The Reference Orbit, Target Site, and Look Vector . . . . .	4-14
4.9.	Minimum $a_e$ Example: Formation Plot with Satellites in RSW	4-15
4.10.	Minimum $a_e$ Example: Formation Plot with Satellites in UV	4-15
4.11.	Three Deputy Example: Possible $a_e$ , $y_d$ Values . . . . .	4-16

Figure		Page
4.12.	Three Deputy Example: Formation Plot with Satellites in RSW	4-16
4.13.	Three Deputy Example: Formation Plot with Satellites in UV	4-17

# *List of Symbols*

Symbol	Page
DSST ... Draper semi-analytic satellite theory . . . . .	1-2
$\vec{r}_{obj}^{XYZ}$ ... Position vector of “obj” in “XYZ” . . . . .	2-1
$\vec{v}_{obj}^{XYZ}$ ... Velocity vector of “obj” in “XYZ” . . . . .	2-1
$\vec{a}_{obj}^{XYZ}$ ... Acceleration vector of “obj” in “XYZ” . . . . .	2-1
$\Xi$ ... Place holder . . . . .	2-1
$\alpha$ ... Explanatory angle . . . . .	2-2
$P$ ... Point of interest . . . . .	2-3
$O'$ ... Origin of the rotating frame . . . . .	2-3
$O$ ... Origin of the fixed frame . . . . .	2-3
$\vec{\omega}$ ... Angular velocity of the rotation frame . . . . .	2-3
$\vec{\alpha}$ ... Angular acceleration of the rotation frame . . . . .	2-3
RSW ... Satellite coordinate frame . . . . .	2-4
BAC ... Relative coordinate frame . . . . .	2-4
IJK ... Earth centered inertial coordinate frame . . . . .	2-4
$\hat{\gamma}$ ... First point of Aries . . . . .	2-4
$La$ ... Latitude . . . . .	2-5
$\Theta_{LST}$ ... Local sidereal time . . . . .	2-5
GMST ... Greenwich mean sidereal time . . . . .	2-5
$lo$ ... longitude . . . . .	2-5
SEZ ... Topocentric horizontal coordinate frame . . . . .	2-5
$az$ ... Azimuth . . . . .	2-5
$el$ ... Elevation . . . . .	2-5
GLP ... Objectcentric viewing coordinate frame . . . . .	2-6
$a_c$ ... Reference (chief) satellite’s semi-major axis . . . . .	2-6
$r_e$ ... Radius of the earth . . . . .	2-6
${}^{SEZ}R^{GLP}$ ... Coordinate transition matrix from GLP to SEZ . . . . .	2-6
$i^{th}$ ... Satellite index . . . . .	2-6
UV ... Observation coordinate frame . . . . .	2-6

Symbol	Page
$D \cdots$ Displacement along the optical axis . . . . .	2-7
$F^3OS \cdots$ Force-Free First-Order Stationary . . . . .	2-7
$C_1 \cdots$ Constant of integration . . . . .	2-12
$C_2 \cdots$ Constant of integration . . . . .	2-13
$z_{max} \cdots$ Relative trajectory magnitude of out of plane oscillation . . .	3-1
$a_e \cdots$ Relative trajectory projected semi-major axis . . . . .	3-1
$y_d \cdots$ Relative trajectory velocity offset . . . . .	3-1
$\beta \cdots$ Parametric angle for deputy location . . . . .	3-1
$\phi \cdots$ Parametric angle to locate deputy's reference plane passage . . .	3-2
$q_r \cdots$ Relative quotient . . . . .	3-6
$a_r \cdots$ Relative trajectory semi-major axis . . . . .	3-6
$b_r \cdots$ Relative trajectory semi-minor axis . . . . .	3-6
$e_r \cdots$ Relative eccentricity . . . . .	3-6
$e \cdots$ Elliptical path designator . . . . .	3-9
$a \cdots$ Auxiliary circle designator . . . . .	3-9
$\tilde{\beta} \cdots$ Physical angle for deputy location . . . . .	3-10
$\tilde{\phi} \cdots$ Parametric angle to locate deputy's reference plane passage . . .	3-11
$\vec{\Omega}_r \cdots$ Relative line of nodes . . . . .	3-12
$\tilde{u}_r \cdots$ Relative argument of latitude . . . . .	3-13
$\mu \cdots$ Kepler's constant . . . . .	4-1
$i_c \cdots$ Reference (chief) satellite's inclination . . . . .	4-1
$L_c \cdots$ Reference (chief) satellite's latitude . . . . .	4-1
$\Omega_c \cdots$ Reference (chief) satellite's right ascending node . . . . .	4-2
$u_c \cdots$ Reference (chief) satellite's argument of latitude . . . . .	4-2
$\hat{n}_r \cdots$ Normal of the relative trajectory plane . . . . .	4-3
$L_r \cdots$ R component of the look vector . . . . .	4-3
$L_s \cdots$ S component of the look vector . . . . .	4-3
$L_w \cdots$ W component of the look vector . . . . .	4-3
$\theta_{error} \cdots$ Perpendicular error . . . . .	4-3
$T_r \cdots$ R component of the target site . . . . .	4-7
$T_s \cdots$ S component of the target site . . . . .	4-7

Symbol	Page
$T_w \cdots$ W component of the target site . . . . .	4-7
$k \cdot$ Intersection index . . . . .	4-10
STK ... Satellite Tool Kit . . . . .	5-1

# GEOMETRIC APPROACH TO ORBITAL FORMATION MISSION DESIGN

## *I. Introduction*

### *1.1 Problem Statement*

A common problem among the space radar community and the space dynamics community is the difficulty in transferring requirements when dealing with satellite arrays. To solve this problem, this thesis examines how to correlate remote sensing requirements with orbital parameters. To insure that these algorithms are operationally practical, analytical solutions, when possible, are developed.

### *1.2 Literature Review*

In the past, looking into the heavens and staring back at Earth was done through the use of expensive and cumbersome satellites. These satellites have been superseded by smaller, more efficient satellites. With this trend, the next evolutionary step has been born: formation flying [20]. Formation flying uses an array of close orbiting small satellites. As Yeh [32] mentions, the term “flying” is somewhat deceiving because it infers the agility of aircraft mobility. Hence, the term orbital formations is used throughout this paper. There are many advantages and uses for orbital formations.

The advantages of orbital formations include a greater flexibility in payload distribution, which increases the launch options thereby reducing the project cost. With the multi-satellite design, it is easier to incorporate redundancy to allow for the system to continue if one satellite fails. In addition, the multiple satellite arrangement makes replacement and upgrading easier. Another advantage directly related to

this thesis is improved and adjustable angular resolution for multi-aperture imaging, where angular resolution is a direct function of the formation geometry.

The potential use for orbital formations widely varies. Several published works have listed possible applications for the orbital formations technology. Johnston [12] and Cornwell [4] name astronomy as a possible use of orbital formations. Others explain how orbital formations could be used for communication, moving target identification [23], and interferometry [4] [6] [13]. Whatever the use, it is important to realize that any performance metric to be achieved by the sensing architecture is a direct function of the formation geometry.

For mission design it is highly advantageous to have an analytical method to calculate the formation geometry. This is somewhat difficult due to the nonlinear, high order, and coupled mathematics [31] [32] that characterize orbital formation dynamics. The approach taken by most authors, including this one, is to use Clohessy and Wiltshire's [3] linearized solutions of Hill's equations [10]. This method does not incorporate any perturbations due to oblateness, therefore it becomes inaccurate for extensive time analysis. However, it is useful for determining the dynamics over shorter periods of time. In fact, Guelman and Aleshin [17] use this method to accurately minimize fuel for rendezvous maneuvers. In addition, Lovell and Tragesser [14] are able to use these solutions to represent reconfiguration maneuvers.

In view of the limitations, several individuals have used their resources to improve upon the Clohessy and Wiltshire model. First order oblateness effects are added to Clohessy and Wiltshire solutions by Schaub and Alfriend [21] who describe the relative orbit using Delaunay [7] orbital elements. Further perturbation effects are added to Clohessy and Wiltshire's solutions by Sedwick, Miller, and Kong [24] who use Buckingham's [2] dimensional equation techniques. The Draper Semi-analytic Satellite Theory (DSST) is used by Sabol, Burns, and McLaughlin [20] to extend the results to include a 21st order gravitational field, lunar and solar third body, atmospheric drag, and solar wind perturbations.



One of the front runners who has taken a drastically different approach to improving the accuracy of dynamic modeling for orbital formations is Wiesel. His method includes tying the typical Gaussian reference used in formation analysis to a Hamiltonian inertial frame, and then, by using the techniques of Floquet [18], analyzing the dynamics of orbital formations. This method increases the accuracy by three or more orders of magnitude beyond what one could expect from Clohessy and Wiltshire's results [31]. This accuracy in calculations is shown through the results arrived at by Bordner [1]. Wiesel expands his work by including second order two-body terms and zonal perturbations into his Floquet analysis [30]. This is expanded by Wiesel's examination of the operational practicality for long term station-keeping [29].

In addition to Wiesel, several others have researched control theory for orbital formations. Yeh, Nelson, and Sparks [32] developed a methodology using a sliding mode framework. Irvin [11] investigated minimal fuel reconfiguration techniques using the Clohessy and Wiltshire solution and a variety of feedback techniques.

The recent interest in orbital formations has increased due to the TechSat 21 program. The TechSat 21 program was an Air Force and NASA feasibility research initiative for satellite formations. This incentive boosted the research in orbital formations design. Great progress was made in the areas of satellite formation dynamics, micro-satellite and micro-propulsion design, distributed mission architecture, sparse aperture sensing, collaborative behavior, and micro-nano-technology [5] [19] [25].

In the last five years a considerable amount of research has been performed on orbital formations. Sabol, Burns, and McLaughlin investigated satellite formation design. Lovell and Tragesser [14] [15] [16] pursued formation reconfiguration and maintenance, whereas Schweighart and Sedwick [22] worked toward a better understanding of relative orbital perturbations. Many others such as Wiesel [29] labored

in this area to improve upon what Clohessy and Wiltshire started in 1960 with their expansion of Hill's 1878 Lunar Theory.

### *1.3 Research Objective*

The objective is to correlate remote sensing requirements to the orbital parameters of stationary satellite formations, and then demonstrate and validate through MATLAB<sup>®</sup> algorithms.

### *1.4 Thesis Outline*

This chapter states the problem explored and reviews previously published literature that gives the reader the background necessary for this study. Chapter II establishes the necessary coordinate system terminology and provides two relevant derivations for insight into the problem and into the limitations of the solution. Chapter III builds upon the characteristics of stationary formations to enhance the design process. Chapter IV sets up the design by providing the necessary inputs, and then correlating points in the imaging plane of a ground site to satellite positions utilizing two distinctly different design constraints. Chapter V provides a summary of the research, the results found, recommendations for future study, and conclusions drawn. Overall, this paper builds upon the concept of the stationary constraint by characterizing the physical relative periodic path. These features are used to correlate basic geometric formation parameters with an instantaneous distribution of satellites as viewed from the ground site imaging plane.

## II. Preliminary Development

### 2.1 Coordinate Systems

Although several authors use cylindrical [28] or spherical coordinates when dealing with formations, in this paper, Cartesian coordinates are used exclusively. All coordinate systems use a right hand rule. The nomenclature for the coordinate systems uses a multi-letter designator where the first letter represents the first axis, the second letter represents the second axis and so forth, until all axes are properly represented. The nomenclature for the position vector of “obj” in the “XYZ” coordinate system will be represented as  $\vec{r}_{obj}^{XYZ}$ , velocity as  $\vec{v}_{obj}^{XYZ}$ , and acceleration as  $\vec{a}_{obj}^{XYZ}$ .

For ease of programming and mathematical manipulation, the position vector may be represented as a 4x1 matrix. Where the first position of the matrix indicates the perpendicular projection of the position vector onto the first axis, the second and third positions follow with the fourth position labelled as  $\Xi$  which is a place holder equivalent to one.

One of the key elements in solving this problem is going from one coordinate system to the next. This makes it imperative that we not only have a good definition of coordinate systems but a reasonable way to change between coordinate systems. To switch between coordinate systems, matrix algebra is used. The three types of 4x4 matrices that are used are rotation matrices, transition matrices, and projection matrices.

There are three types of rotation matrices. Each of these rotation matrices rotates the system clockwise as viewed from the negative axis. The One Rotation

refers to a rotation of  $\alpha$  degrees about the first axis,

$$ROT1(\alpha) = \begin{bmatrix} 1 & 0 & 0 & 0 \\ 0 & \cos(\alpha) & \sin(\alpha) & 0 \\ 0 & -\sin(\alpha) & \cos(\alpha) & 0 \\ 0 & 0 & 0 & 1 \end{bmatrix} \quad (2.1)$$

and the MATLAB<sup>®</sup> code can be seen in Appendix(B). The Two Rotation refers to a rotation about the second axis of  $\alpha$  degrees,

$$ROT2(\alpha) = \begin{bmatrix} \cos(\alpha) & 0 & -\sin(\alpha) & 0 \\ 0 & 1 & 0 & 0 \\ \sin(\alpha) & 0 & \cos(\alpha) & 0 \\ 0 & 0 & 0 & 1 \end{bmatrix} \quad (2.2)$$

and the MATLAB<sup>®</sup> code can be seen in Appendix(C). The Three Rotation refers to a rotation of  $\alpha$  degrees about the third axis,

$$ROT3(\alpha) = \begin{bmatrix} \cos(\alpha) & \sin(\alpha) & 0 & 0 \\ -\sin(\alpha) & \cos(\alpha) & 0 & 0 \\ 0 & 0 & 1 & 0 \\ 0 & 0 & 0 & 1 \end{bmatrix} \quad (2.3)$$

and the MATLAB<sup>®</sup> code can be seen in Appendix(D).

There is one general translation matrix that will be used, and it has the following form.

$$TRAN(\Delta x, \Delta y, \Delta z) = \begin{bmatrix} 1 & 0 & 0 & \Delta x \\ 0 & 1 & 0 & \Delta y \\ 0 & 0 & 1 & \Delta z \\ 0 & 0 & 0 & 1 \end{bmatrix} \quad (2.4)$$

Where  $\Delta x$  is a translation along the first axis,  $\Delta y$  is a translation along the second axis, and  $\Delta z$  is a translation along the third axis.

Mapping from three dimensions onto two dimensions is called perspective projection. The matrix that performs the perspective projection is shown in section 2.1.6.

The transformation of velocity and acceleration vectors is slightly different due to the motion of frames. The relationship between the inertial velocity and relative velocity is

$$\vec{v}_P = \vec{v}_{O'} + \vec{v}_{rel} + \vec{\omega} \times \vec{r}_{P/O'} \quad (2.5)$$

Where the subscript  $P$  represents the point of interest,  $O'$  represents the origin of the rotating frame, and  $O$  represents the fixed reference frame.  $\vec{r}_{P/O'}$  describes point  $P$  as seen from the moving reference frame and  $\vec{\omega}$  is the angular velocity of the rotation frame. The relationship between the inertial acceleration and relative acceleration is

$$\vec{a}_P = \vec{a}_{O'} + \vec{a}_{rel} + \vec{\alpha} \times \vec{r}_{P/O'} + \vec{\omega} \times (\vec{\omega} \times \vec{r}_{P/O'}) + 2\vec{\omega} \times \vec{v}_{rel} \quad (2.6)$$

where  $\vec{\alpha}$  is the angular acceleration of the rotation frame. The three general types of acceleration can be seen in the equation above. The Coriolis acceleration is

$$\vec{a}_{cor} = 2\vec{\omega} \times \vec{v}_{rel} \quad (2.7)$$

The centripetal acceleration is

$$\vec{a}_{cen} = \vec{\omega} \times (\vec{\omega} \times \vec{r}_{P/O'}) \quad (2.8)$$

The tangential acceleration is

$$\vec{a}_{tan} = \vec{\alpha} \times \vec{r}_{P/O'} \quad (2.9)$$

By assuming a circular orbit, the tangential acceleration is zero. Therefore, the inertial acceleration may be related to the relative acceleration by

$$\vec{a}_P = \vec{a}_{O'} + \vec{a}_{rel} + \vec{\omega} \times (\vec{\omega} \times \vec{r}_{P/O'}) + 2\vec{\omega} \times \vec{v}_{rel} \quad (2.10)$$

*2.1.1 Satellite “RSW”.* The RSW coordinate system is a rotating coordinate system whose origin is a reference satellite. The reference satellite is referred to as the chief. As the chief moves through its circular orbit,  $\hat{R}$  is in the direction of the chief’s position vector,  $\hat{S}$  is in the direction of the chief’s velocity, and  $\hat{W}$  is normal to the chief’s orbital plane. For the purpose of this paper, x, y, and z depict the position of a secondary or deputy satellite’s R, S, and W components respectively. MATLAB<sup>®</sup> code to perform coordinate transformation is found in Appendix(H).

*2.1.2 Relative “BAC”.* Another coordinate system whose value and orientation will become clear later is the Relative Stationary Orbital coordinate system, BAC, where the origin is located at the “pseudo-chief”, the center of the deputies elliptical trajectory as explained in Section 3.2, and the B-axis is in the direction of the semi-minor axis in the positive direction of  $\hat{W}$  of the RSW frame. The A-axis is in the direction of the semi-major axis, and  $\hat{C}$  is normal to the relative formation plane. Figure 2.1 illustrates the BAC coordinate system.

*2.1.3 Earth Centered Inertial “IJK”.* The Earth Centered Inertial coordinate system, IJK, is the inertial frame for this paper. As suggested by the title, this is a geocentric coordinate system, or in other words the origin is at the center of the earth. The I-J plane passes through the earth’s equator. The I-axis points towards the vernal equinox. The direction of the vernal equinox is designated  $\hat{\gamma}$  and is often referred to as the first point of Aries but points in the direction of the constellation Pisces. The J-axis is located 90 ° from  $\hat{I}$  in the direction of the earth’s rotation, and the K-axis points toward the North Pole. A point on the earth, target site, may be

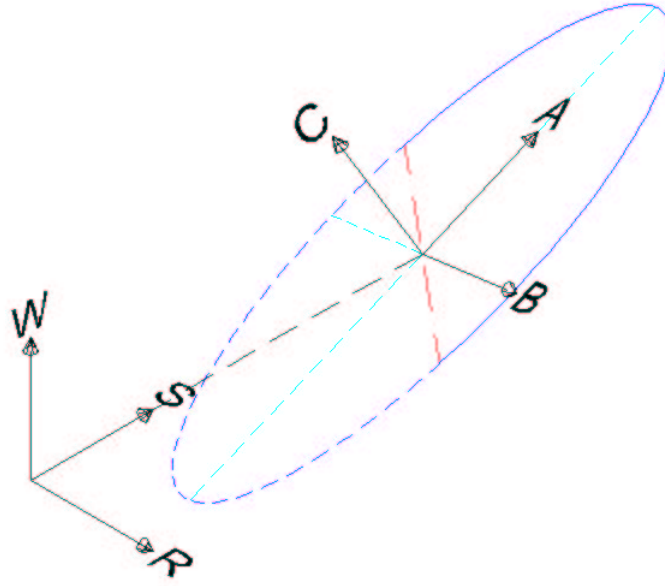


Figure 2.1 “BAC” Coordinate System

located by the two angles  $La$  and  $\Theta_{LST}$ . The latitude,  $La$ , is an angle from the I-J plane, whereas  $\Theta_{LST}$  is an angle from the I-axis in the direction of the rotation of the earth.  $\Theta_{LST}$  is equal to the GMST, Greenwich Mean Sidereal Time, angle plus  $lo$ , the longitude. MATLAB<sup>®</sup> code to perform coordinate transformation is found in Appendixes (H) and (I).

*2.1.4 Topocentric Horizontal “SEZ”.* The SEZ system’s origin rotates with the target site. The target site location is calculated using a spherical earth. The S-axis points directly south from the site. The E-axis points east from the site. The Z-axis points radially outward from the center of the earth. The direction of an object viewed from SEZ will be located with a look vector where the look vector is defined by an azimuth,  $az$ , and elevation angle,  $el$ . Azimuth is the angle measured from the negative S-axis (North) clockwise as viewed from above the site to the location beneath the location of interest and can be values from 0 to 360 degrees. Elevation is measured from the local horizon position in the direction of positive zenith to the object of interest. Elevation can take on values between 0 and 90 degrees. MATLAB<sup>®</sup> code to perform coordinate transformation is found in Appendixes (I) and (J).

*2.1.5 Objectcentric Viewing “GLP”.* It is beneficial to establish an intermediate coordinate system, GLP, to differentiate between points that exist in three-dimensional space and those that are simply projections of points. The GLP coordinate system’s origin is displaced from the origin of the SEZ frame in the reference satellite’s positive look vector direction. To abbreviate the problem, the distance the origin is displaced is assumed to be equivalent to the reference satellite’s range. The assumption that the displacement of the origin is equivalent to the range makes the GLP coordinate system an objectcentric imaging coordinate system whose origin is the chief satellite. The range may simply be defined by the chief’s radius,  $a_c$  (characterized by the chief’s period), and elevation angle:

$$\rho = \sqrt{a_c^2 - r_e^2 \cdot \cos(el)^2} - r_e \cdot \sin(el) \quad (2.11)$$

where  $r_e$  is the radius of the earth.  $\hat{G}$  is parallel to the Ground (S-E plane).  $\hat{L}$  is in the direction of the Look vector, and  $\hat{P}$  is defined in the Positive zenith direction (see Figure 2.2). The translation and rotation matrix for GLP to SEZ,  $^{SEZ}R^{GLP}$ , is

$$ROT3(az - \frac{\pi}{2}) \cdot ROT1(-el) \cdot TRAN(0, \rho, 0) \quad (2.12)$$

MATLAB<sup>®</sup> code to perform this coordinate transformation is found in Appendix (K).

*2.1.6 Observation “UV”.* The axes of the imaging plane are  $\hat{U}$  and  $\hat{V}$ , where  $\hat{U}$  is in the G direction, and, atypical from convention,  $\hat{V}$  is in the positive P direction. The objective is to correlate each satellite in an array to a specific observation point on the u-v plane, so that the location of the  $i^{th}$  satellite is specified by  $(u_i, v_i)$ . Mapping from three dimensions onto two dimensions is called perspective projection. The projection matrix for GLP to UV,  $^{UV}R^{GLP}$ , is

$$\begin{bmatrix} \frac{\rho}{D+\rho} & 0 & 0 & 0 \\ 0 & \frac{\rho}{D+\rho} & 0 & 0 \end{bmatrix} \quad (2.13)$$

2-6



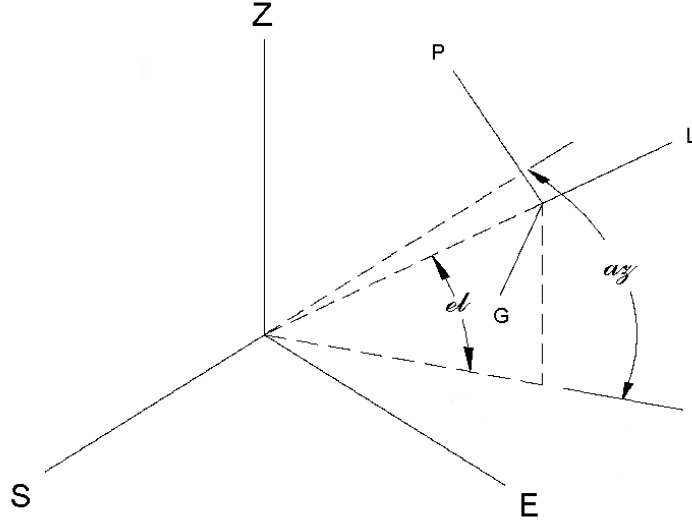


Figure 2.2 “GLP” Coordinate System

where  $D$  represents the distance along the optical axis. The optical axis is  $\hat{L}$  of the GLP coordinate system. MATLAB<sup>®</sup> code to perform coordinate transformation is found in Appendix (K).

## 2.2 Preliminary Equations

A common set of relative motion equations used in orbital formation analysis is Hill’s equations. Several texts, including Wiesel [28], have derivations of Hill’s equations. To explicitly illustrate the various assumptions on which this paper is based, Hill’s equations are developed from the force-free first-order linearization of the point mass two body motion equation. This is followed by the solution of Hill’s equations using the stationary constraint to form the force-free first-order stationary (F<sup>3</sup>OS) formation equations.

*2.2.1 Hill's Equations.* The equation of motion for the reference satellite, or chief, is defined using the point mass two-body motion equation.

$$\ddot{\vec{r}}_c = -\frac{\mu \cdot \vec{r}_c}{r_c^3} \quad (2.14)$$

Considering no additional forces on the deputy satellite, i.e., force-free, the equation of motion for the deputy is given as

$$\ddot{\vec{r}}_d = -\frac{\mu \cdot \vec{r}_d}{r_d^3} \quad (2.15)$$

The relative position vector is defined as

$$\vec{r}_r = \vec{r}_d - \vec{r}_c \quad (2.16)$$

Using Eq.(2.16), the deputy position is

$$\vec{r}_d = \vec{r}_c + \vec{r}_r \quad (2.17)$$

Using the cosine law by definition of the dot product:

$$|\vec{r}_1 - \vec{r}_2|^2 = \vec{r}_1 \bullet \vec{r}_1 - 2 \cdot \vec{r}_1 \bullet \vec{r}_2 + \vec{r}_2 \bullet \vec{r}_2 \quad (2.18)$$

the magnitude of the deputy's position is

$$r_d = \sqrt{r_c^2 + 2 \cdot \vec{r}_c \bullet \vec{r}_r + r_r^2} \quad (2.19)$$

Cubing Eq.(2.19) and using Eq.(2.17) yields

$$\frac{r_d^3}{r_d^3} = \frac{r_c^3 + r_r^3}{(r_c^2 + 2\vec{r}_c \bullet \vec{r}_r + r_r^2)^{\frac{3}{2}}} \quad (2.20)$$

It is assumed that the square of the distance between the chief and deputy is small compared to the magnitude of the chief's position vector squared. Through this assumption, Eq.(2.20) may be rearranged.

$$\frac{\vec{r}_d}{r_d^3} = \frac{\vec{r}_c + \vec{r}_r}{r_c^3} \left( 1 + \frac{2\vec{r}_c \bullet \vec{r}_r}{r_c^2} \right)^{-3/2} \quad (2.21)$$

Use the binomial series:

$$(1 + x)^n = 1 + nx + \frac{n(n-1)x^2}{2!} + \dots \quad (2.22)$$

to expand the second part of Eq.(2.21) where

$$x = \frac{2\vec{r}_c \bullet \vec{r}_r}{r_c^2} \quad n = \frac{-3}{2} \quad (2.23)$$

yields

$$\frac{\vec{r}_d}{r_d^3} = \frac{\vec{r}_c + \vec{r}_r}{r_c^3} \left\{ 1 - \frac{3}{2} \left( \frac{2\vec{r}_c \bullet \vec{r}_r}{r_c^2} \right) + \dots \right\} \quad (2.24)$$

Differentiating Eq.(2.16) twice yields

$$\ddot{\vec{r}}_r = \ddot{\vec{r}}_d - \ddot{\vec{r}}_c \quad (2.25)$$

Substituting Eq.(2.14) and Eq.(2.15) yields

$$\ddot{\vec{r}}_r = \frac{-\mu\vec{r}_d}{r_d^3} + \frac{\mu\vec{r}_c}{r_c^3} \quad (2.26)$$

Substituting Eq.(2.24) results in

$$\ddot{\vec{r}}_r = -\mu \left( \frac{\vec{r}_c + \vec{r}_r}{r_c^3} \cdot \left\{ 1 - \frac{3}{2} \left( \frac{2\vec{r}_c \bullet \vec{r}_r}{r_c^2} \right) + \dots \right\} \right) + \frac{\mu\vec{r}_c}{r_c^3} \quad (2.27)$$

Eliminating all second order or greater terms (hence the term first-order equation) and simplifying yields

$$\ddot{\vec{r}}_r = -\frac{\mu}{r_c^3} \left( -\frac{3\vec{r}_c}{2} \left( \frac{2\vec{r}_c \bullet \vec{r}_r}{r_c^2} \right) + \vec{r}_r - \frac{3\vec{r}_r}{2} \left( \frac{2\vec{r}_c \bullet \vec{r}_r}{r_c^2} \right) \right) \quad (2.28)$$

The assumption is made that  $\vec{r}_r/r_c^2$  is very small and therefore may be set to zero. This provides the equation of the inertial acceleration of the deputy in the RSW frame.

$$\ddot{\vec{r}}_r = -\frac{\mu}{r_c^3} \left( -\frac{3\vec{r}_c}{2r_c} \left( \frac{2\vec{r}_c \bullet \vec{r}_r}{r_c} \right) + \vec{r}_r \right) \quad (2.29)$$

The relative position in the RSW frame may be defined as

$$\vec{r}_r = x \cdot \hat{R} + y \cdot \hat{S} + z \cdot \hat{W} \quad (2.30)$$

By definition of the RSW frame,  $\vec{r}_c$  is in the direction of  $\hat{R}$ .

$$\vec{r}_c = r_c \cdot \hat{R} \quad (2.31)$$

Using Kepler's third law, the mean motion of the circular orbit is

$$\omega = \sqrt{\frac{\mu}{r_c^3}} \quad (2.32)$$

Therefore using Eqs.(2.30) and (2.32), Eq.(2.29) may be simplified to

$$\ddot{\vec{r}}_r = -\omega^2 \left( -3x\hat{R} + \left( x \cdot \hat{R} + y \cdot \hat{S} + z \cdot \hat{W} \right) \right) \quad (2.33)$$

The mean motion vector of the reference satellite is about the W-axis, and therefore may be represented as

$$\vec{\omega} = \omega \cdot \hat{W} \quad (2.34)$$

The Coriolis acceleration is found using Eqs.(2.7) and (2.34) in addition to the derivative of Eq.(2.30).

$$a_{cor}^{\vec{}} = 2 \left( -\omega \dot{y} \hat{R} + \omega \dot{x} \hat{S} \right) \quad (2.35)$$

Using Eqs.(2.8), (2.30), and (2.34), the centripetal acceleration is

$$a_{cen}^{\vec{}} = -\omega^2 x \hat{R} - \omega^2 y \hat{S} \quad (2.36)$$

Substituting Eqs.(2.33), (2.35), and (2.36) into Eq.(2.10) and solving for the relative acceleration yields

$$\ddot{\vec{r}}_{rR} = -\omega^2 \left( -3x \hat{R} + \left( x \cdot \hat{R} + y \cdot \hat{S} + z \cdot \hat{W} \right) \right) - 2 \left( -\omega \dot{y} \hat{R} + \omega \dot{x} \hat{S} \right) + \omega^2 x \hat{R} + \omega^2 y \hat{S} \quad (2.37)$$

Writing each vector component separately yields Hill's force-free first-order equations:

$$\ddot{x} = 3 \cdot \omega^2 \cdot x + 2 \cdot \omega \cdot \dot{y} \quad (2.38)$$

$$\ddot{y} = -2 \cdot \omega \cdot \dot{x} \quad (2.39)$$

$$\ddot{z} = -\omega^2 \cdot z \quad (2.40)$$

*2.2.2 Hill's Stationary Solution.* Many methods are available to solve Hill's equations. One of the more common methods employs Laplace operators, as are used here to follow Vallado's derivation. Begin by taking the derivative of Eq.(2.38).

$$\ddot{x} = 3\omega^2 \dot{x} + 2\omega \ddot{y} \quad (2.41)$$

Substituting Eq.(2.39) and simplifying yields

$$\ddot{x} + \omega^2 \dot{x} = 0 \quad (2.42)$$

Therefore, the Laplace transform is

$$\mathcal{L} [\ddot{x} + \omega^2 \dot{x}] = \{s^3 X(s) - s^2 x_0 - s \dot{x}_0 - \ddot{x}_0\} + \omega^2 \{s X(s) - x_0\} = 0 \quad (2.43)$$

The solution of the subsidiary equation is

$$X(s) = \frac{x_0}{s} + \frac{\dot{x}_0}{(s^2 + \omega^2)} + \frac{\ddot{x}_0}{s\omega^2} - \frac{s\ddot{x}_0}{\omega^2(s^2 + \omega^2)} \quad (2.44)$$

Taking it back into the time domain through the inverse Laplace yields

$$x(t) = x_0 + \frac{\ddot{x}_0}{\omega^2} + \frac{\dot{x}_0}{\omega} \sin(\omega t) - \frac{\ddot{x}_0}{\omega^2} \cos(\omega t) \quad (2.45)$$

Substituting Eq.(2.38) into the equation above and simplifying leads to

$$x(t) = 4x_0 + \frac{2\dot{y}_0}{\omega} + \frac{\dot{x}_0}{\omega} \sin(\omega t) - \left(3x_0 + \frac{2\dot{y}_0}{\omega}\right) \cos(\omega t) \quad (2.46)$$

Differentiating with respect to time yields

$$\dot{x}(t) = \dot{x}_0 \cos(\omega t) + (3\omega x_0 + 2\dot{y}_0) \sin(\omega t) \quad (2.47)$$

Substituting the above equation into Eq.(2.39) and simplifying gives

$$\ddot{y} = -2\omega \dot{x}_0 \cos(\omega t) - 2\omega(3\omega x_0 + 2\dot{y}_0) \sin(\omega t) \quad (2.48)$$

Integrating yields

$$\dot{y} = -2\dot{x}_0 \sin(\omega t) + 2(3\omega x_0 + 2\dot{y}_0) \cos(\omega t) + C_1 \quad (2.49)$$

where  $C_1$  is a constant of integration. Integrating a second time yields

$$y = \frac{2\dot{x}_0}{\omega} \cos(\omega t) + \left(6x_0 + \frac{4\dot{y}_0}{\omega}\right) \sin(\omega t) + C_1 t + C_2 \quad (2.50)$$

From the second constant of integration,  $C_2$ , it may be seen that the position in the y direction has a constant offset, later termed  $y_d$ . The first constant of integration is multiplied by time, thereby indicating that the y component of the relative position of the deputy satellite will vary with time. This variation with time has been termed “drift”. A stationary formation is one with no drift, i.e.,  $C_1 = 0$ . To solve for the first constant of integration in terms of initial conditions, Eq.(2.49) is evaluated at the initial time,  $t = 0$ .

$$\dot{y}_0 = 6\omega x_0 + 4y_0 + C_1 \quad (2.51)$$

The stationary constraint is found by setting  $C_1 = 0$  and simplifying.

$$\dot{y}_o = -2 \cdot \omega \cdot x_o \quad (2.52)$$

By inducing the stationary constraint, the motion of the deputy is contained to a periodic elliptical path, and the total number of undetermined states is reduced from six to five. To solve for the second constant of integration, Eq.(2.50) is evaluated at  $t = 0$ .

$$C_2 = -\frac{2\dot{x}_0}{\omega} + y_0 \quad (2.53)$$

This leads to the y position equation for F<sup>3</sup>OS formations.

$$y(t) = 2 \cdot \frac{\dot{x}_o}{\omega} \cdot \cos(\omega \cdot t) - 2 \cdot x_o \cdot \sin(\omega \cdot t) + y_o - 2 \cdot \frac{\dot{x}_o}{\omega} \quad (2.54)$$

As Vallado [26] mentions, Eq.(2.38) and Eq.(2.39) are coupled, therefore the stationary constraint must also be applied to Eq.(2.46) yielding the x position equation for F<sup>3</sup>OS formations.

$$x(t) = \frac{\dot{x}_o}{\omega} \cdot \sin(\omega \cdot t) + x_o \cdot \cos(\omega \cdot t) \quad (2.55)$$

As stated in Wiesel [28], the solution to the z equation is a simple harmonic oscillator given by

$$\ddot{z} + \omega^2 z = 0 \quad (2.56)$$

and when transformed using Laplace, follows

$$s^2 Z(s) - sz_0 - \dot{z}_0 + \omega^2 Z(s) = 0 \quad (2.57)$$

$$Z(s)(s^2 + \omega^2) = sz_0 + \dot{z}_0 \quad (2.58)$$

$$Z(s) = \frac{sz_0}{(s^2 + \omega^2)} + \frac{\dot{z}_0}{(s^2 + \omega^2)} \quad (2.59)$$

The derivation is completed by using the inverse Laplace to obtain the z position equation for F<sup>3</sup>OS formations.

$$z(t) = z_0 \cos(\omega t) + \frac{\dot{z}_0}{\omega} \sin(\omega t) \quad (2.60)$$

Therefore Eqs.(2.54), (2.55), and (2.60) are termed the F<sup>3</sup>OS equations. These equations are the solutions to Eqs.(2.38), (2.39), and (2.40), Hill's force-free first-order equations, when Eq.(2.52), the stationary constraint, is enforced.



### III. Stationary Formation Characteristics

#### 3.1 Parameterization

Through simple examination of Eq.(2.54) and Eq.(2.55), it can be seen that magnitude of oscillation in the velocity direction is twice that of the radial direction. This magnitude gives the semi-major axis of the in-plane,  $R$ - $S$  plane, ellipse which was discussed by Sabol [20] and is defined here by

$$a_e = 2 \cdot \sqrt{\left(\frac{\dot{x}_o}{\omega}\right)^2 + x_o^2} \quad (3.1)$$

The constant terms found in the  $y(t)$  equation of Eq.(2.54) are represented by  $y_d$  which has the physical significance of being the displacement of the center of the formation in the velocity ( $\hat{S}$ ) direction.

$$y_d = y_o - 2 \cdot \left(\frac{\dot{x}_o}{\omega}\right) \quad (3.2)$$

By examining Eq.(2.60), the amplitude of oscillation in the  $z(t)$ , or the out-of-plane direction, is termed  $z_{max}$  and is defined as

$$z_{max} = \sqrt{\left(\frac{\dot{z}_o}{\omega}\right)^2 + z_o^2} \quad (3.3)$$

Figure 3.1 gives a physical representation of the parameterization variables  $a_e$ ,  $y_d$ , and  $z_{max}$ . Using Lovell's [14] notation and convention, the variable  $\beta$  is a parametric angle in the chief's orbital plane measured from the negative  $R$ -axis in the direction of motion to locate the deputy.

$$\beta = \omega \cdot t + \beta_o \quad (3.4)$$

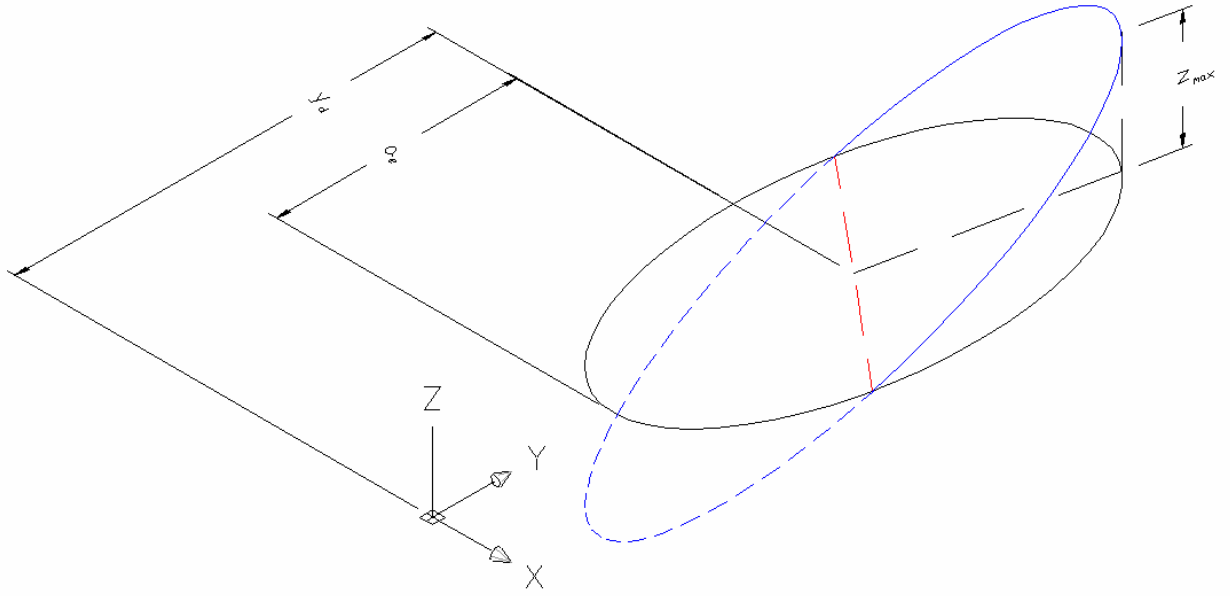


Figure 3.1 Physical Representation of  $a_e$ ,  $z_{max}$  and  $y_d$

where

$$\beta_o = \tan^{-1} \left( \frac{-\dot{x}_o}{\omega \cdot x_o} \right) \quad (3.5)$$

The phasing of  $z(t)$  is adjusted using the parameter  $\phi$ . Varying from Lovell [14], this parametric angle is given by

$$\phi = \beta_o - \tan^{-1} \left( \frac{\dot{z}_o}{\omega \cdot z_o} \right) \quad (3.6)$$

related to an in-plane physical angle measured from perigee to the point at which the satellite ascends through the reference orbital plane. The solution to Hill's equations is re-parameterized utilizing Eqs.(3.1)-(3.6). The relative position is then described

by

$$x = \frac{-a_e}{2} \cdot \cos(\beta) \quad (3.7)$$

$$y = a_e \cdot \sin(\beta) + y_d \quad (3.8)$$

$$z = z_{\max} \cdot \sin(\beta - \phi) \quad (3.9)$$

Note that  $\beta - \phi$  in Eq.(3.9) indicates the phase of the deputy's motion in the  $\hat{W}$  direction.

### 3.2 Formation Plane

The result of manipulating Eq.(3.7) is

$$\cos(\beta) = \frac{-2 \cdot x}{a_e} \quad (3.10)$$

and rearranging Eq.(3.8) gives

$$\sin(\beta) = \frac{y - y_d}{a_e} \quad (3.11)$$

Substituting Eqs.(3.10) and (3.11) into the trigonometric identity  $\sin(\beta)^2 + \cos(\beta)^2 = 1$  results in

$$\frac{4 \cdot x^2}{a_e^2} + \frac{(y - y_d)^2}{a_e^2} = 1 \quad (3.12)$$

which is an elliptical cylinder with an eccentricity of  $\sqrt{3}/2$ . The deputy satellite must always lie on this cylinder. This agrees with Sabol's [20] statement of a 2x1 in-plane projected ellipse having the semi-major axis in the velocity direction. Using the angle difference relationship, Eq.(A.18), to expand Eq.(3.9), results in

$$z = z_{\max} \cdot (\sin(\beta) \cdot \cos(\phi) - \cos(\beta) \cdot \sin(\phi)) \quad (3.13)$$

Substituting Eqs.(3.10) and (3.11) into Eq.(3.13) results in

$$z = z_{\max} \cdot \left( \left( \frac{y - y_d}{a_e} \right) \cdot \cos(\phi) - \left( \frac{-2 \cdot x}{a_e} \right) \cdot \sin(\phi) \right) \quad (3.14)$$

and simplifies to

$$2 \cdot \sin(\phi) \cdot \left( \frac{z_{\max}}{a_e} \right) \cdot x + \cos(\phi) \cdot \left( \frac{z_{\max}}{a_e} \right) \cdot y + -z = \cos(\phi) \cdot \left( \frac{z_{\max}}{a_e} \right) \cdot y_d \quad (3.15)$$

When  $y_d = 0$ , the normal of the relative trajectory is identified as

$$\vec{n}_r = \begin{bmatrix} 2 \cdot \sin(\phi) \\ \cos(\phi) \\ \frac{-a_e}{z_{\max}} \end{bmatrix} \quad (3.16)$$

Therefore, the formation plane is defined as

$$\begin{bmatrix} 2 \cdot \sin(\phi) \\ \cos(\phi) \\ \frac{-a_e}{z_{\max}} \end{bmatrix} \bullet \begin{pmatrix} x \\ y \\ z \end{pmatrix} = 0 \quad (3.17)$$

The deputy's trajectory is thus defined as the intersection of an elliptical cylinder and a plane, where the former is defined by  $a_e$  and  $y_d$  and the latter by  $\phi$ ,  $a_e$ , and  $z_{\max}$ . Furthermore, the intersection of an elliptical cylinder and a plane can be shown to be an ellipse [8] [9]. To the author's knowledge, this is the first time in literature that the relative path of a stationary formation is proven to have an elliptical trajectory.

### 3.3 Relative Axis

With the plane defined, the major and minor axis of the relative ellipse are now found. First, the distance from the center of the ellipse, pseudo-chief, to the deputy is given by

$$d(t) = \sqrt{x^2 + y^2 + z^2} \quad (3.18)$$

Substituting the stationary equations, Eqs.(3.7)-(3.9), into Eq.(3.18) yields

$$d(t) = \sqrt{\frac{a_e^2}{4} \cdot \cos(\beta)^2 + a_e^2 \cdot \sin(\beta)^2 + z_{\max}^2 \cdot \sin(\beta - \phi)^2} \quad (3.19)$$

Differentiating Eq.(3.19) with respect to  $\beta$  and then setting the numerator of the derivative equal to zero gives an equation governing the location of the minimum and maximum distance:

$$3 \cdot a_e^2 \cdot \cos(\beta) \cdot \sin(\beta) + 4 \cdot z_{\max}^2 \cdot \cos(\beta - \phi) \cdot \sin(\beta - \phi) = 0 \quad (3.20)$$

where  $\beta^*$  is the value of  $\beta$  corresponding to the extrema of  $d(t)$ . Expanding  $\cos(\beta^* - \phi)$  and  $\sin(\beta^* - \phi)$  and performing algebra yields

$$2 \cdot \cos(\phi)^2 + \frac{\cos(\phi) \cdot \sin(\phi)}{\cos(\beta^*) \cdot \sin(\beta^*)} - 2 \cdot \frac{\cos(\beta^*)}{\sin(\beta^*)} \cdot \cos(\phi) \cdot \sin(\phi) - 1 = \frac{-3 \cdot a_e^2}{4 \cdot z_{\max}^2} \quad (3.21)$$

This allows  $\beta^*$  to be isolated on the left side of the equation and the right side to be a function of  $a_e$ ,  $z_{\max}$ , and  $\phi$ .

$$\frac{2 \cdot \cos(\beta^*)^2 - 1}{\cos(\beta^*) \cdot \sin(\beta^*)} = \left( \frac{3 \cdot a_e^2}{4 \cdot z_{\max}^2} + 2 \cdot \cos(\phi)^2 + 1 \right) \cdot (\cos(\phi) \cdot \sin(\phi))^{-1} \quad (3.22)$$

Through additional algebra and trigonometric substitutions, this equation is put into the polynomial form:

$$\cos(\beta^*)^4 - \cos(\beta^*)^2 = \frac{16 \cdot (\cos(\phi)^2 - \cos(\phi)^4) \cdot \left( \frac{z_{\max}}{a_e} \right)^4}{\left[ (128 \cdot \cos(\phi)^2 + 16) \cdot \left( \frac{z_{\max}}{a_e} \right)^4 + (48 \cdot \cos(\phi)^2 + 24) \cdot \left( \frac{z_{\max}}{a_e} \right)^2 + 9 \right]} \quad (3.23)$$

Noting that  $z_{\max}$  and  $a_e$  appear as a ratio (confirmed in Section 3.5), the relative quotient is defined as

$$q_r = \frac{z_{\max}}{a_e} \quad (3.24)$$

Through use of the quadratic formula, a solution of  $\cos(\beta^*)^2$  is attained and further resolved to find four solutions of  $\beta^*$  as a function of  $q_r$  and  $\phi$ .

$$\beta^* = \cos^{-1} \left( \pm \sqrt{\frac{1 \pm \sqrt{\frac{(16+192 \cdot \cos(\phi)^2 - 64 \cdot \cos(\phi)^4) \cdot q_r^4 + (24+48 \cdot \cos(\phi)^2) \cdot q_r^2 + 9}{(16+128 \cdot \cos(\phi)^2) \cdot q_r^4 + (24+48 \cdot \cos(\phi)^2) \cdot q_r^2 + 9}}}{2}} \right) \quad (3.25)$$

Assuming that  $\beta^*$  is a positive angle, the solution is reduced to two values. These two values for  $\beta^*$  can then be placed into Eq.(3.19) to find the magnitude of the semi-major axis,  $a_r$ , and semi-minor axis,  $b_r$ , respectively or into Eqs.(3.7)-(3.9) to find the position of these points,  $\vec{a}_r$  and  $\vec{b}_r$ , relative to the chief. It can be shown that the direction of  $\vec{a}_r$  is a function of  $q_r$  and  $\phi$ , while  $a_r$  is a function of  $z_{max}$ ,  $\phi$ , and a linear relationship with  $a_e$ . The same dependence holds for  $\vec{b}_r$  and  $b_r$ . Figure 3.2 gives a physical representation of the semi-major and semi-minor axis of the elliptical trajectory.

### 3.4 Relative Eccentricity

The relative eccentricity may now be defined as

$$e_r = \sqrt{1 - \frac{b_r^2}{a_r^2}} \quad (3.26)$$

in which the ratio  $b_r/a_r$  is only a function of  $q_r$  and  $\phi$  as plotted in Figures 3.3 and 3.4.

For  $0^\circ < \phi < 360^\circ$ , there are only two cases in which the relative eccentricity,  $e_r$ , equals zero. They occur at  $\phi = \pi/2$ , as appears in Figure 3.3, and  $\phi = 3 \cdot \pi/2$ . This is consistent with Lovell's circular formation [14]. It is important to note from Figure 3.4 that for a given  $\phi$ , there exists a minimal achievable relative eccentricity.

*3.4.1 Example.* For example, if a 2x1 elliptical formation is desired, simply set  $a_r/b_r = 2$ , where  $a_r$  and  $b_r$  are computed by evaluating Eq.(3.19) at the appro-

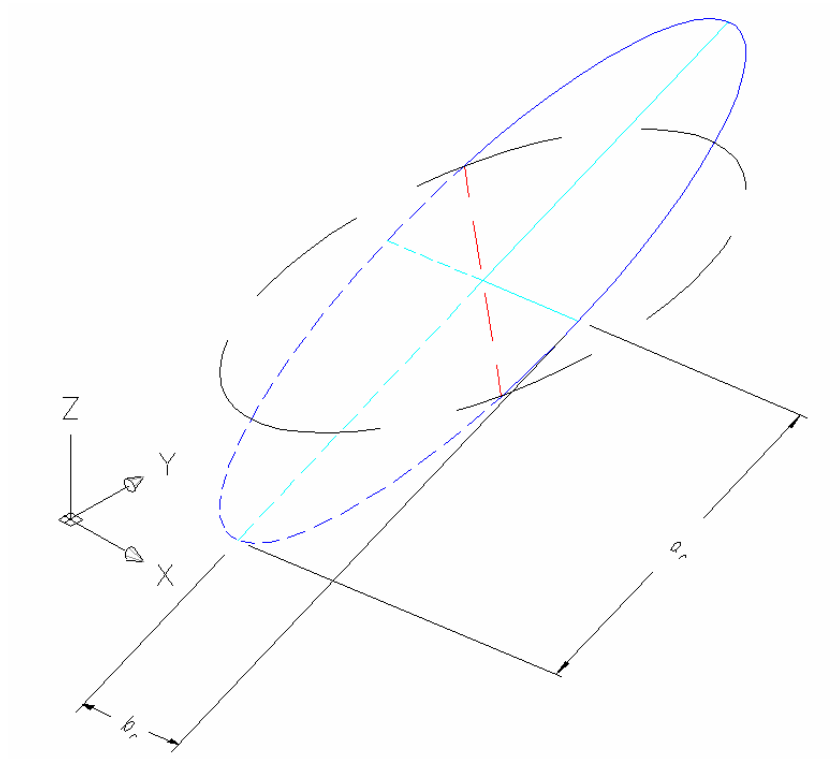


Figure 3.2 Physical Representation of  $a_r$  and  $b_r$

priate  $\beta^*$  given by Eq.(3.25). This particular case is chosen because the resulting simplification is comparatively uncomplicated.

$$a_e = \frac{4 \cdot z_{\max}}{\sqrt{-15 + 75 \cdot \sin(\phi)^2}} \quad (3.27)$$

Therefore, for a given value of  $z_{\max}$ , only one value of  $a_e$  provides the desired eccentricity. Furthermore, not all values of  $\phi$  are possible. The results are imaginary for  $\phi$  between 0 and  $\sin^{-1}(1/\sqrt{5})$ , and the relative quotient as a function of  $\phi$  appears as

$$q_r = \frac{\sqrt{-15 + 75 \cdot \sin(\phi)^2}}{4} \quad (3.28)$$

For this case, the minimum  $\phi$  may be defined as

$$\phi_{\min} = \sin^{-1}\left(\frac{1}{\sqrt{5}}\right) \approx 26.565^\circ \quad (3.29)$$

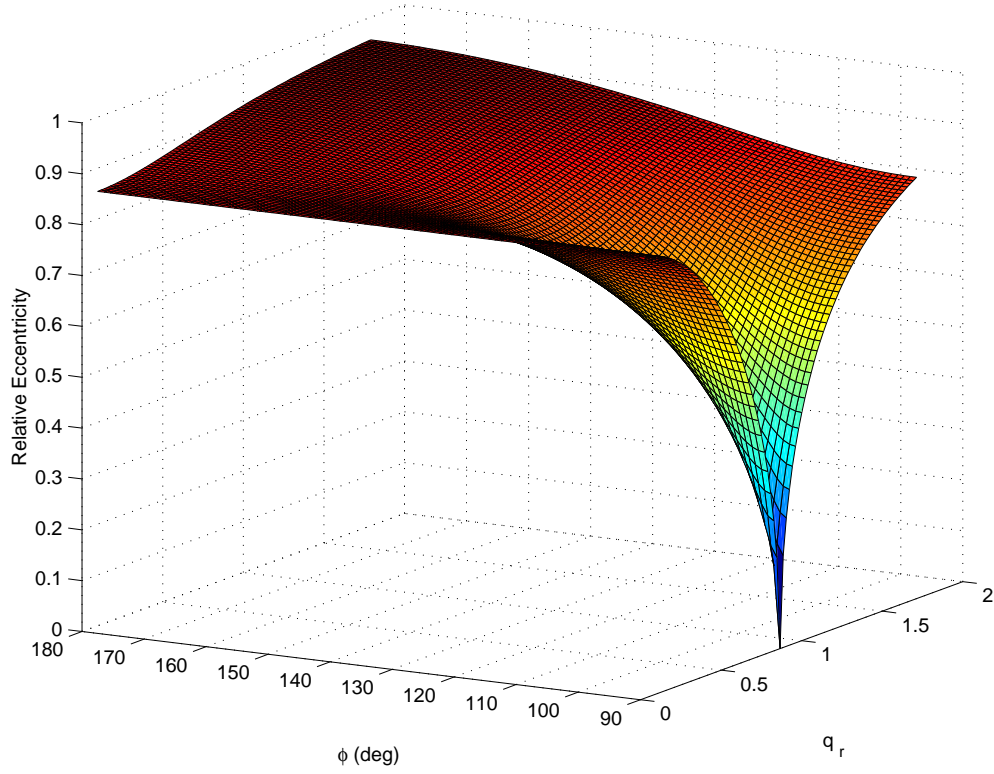


Figure 3.3 Eccentricity Versus  $q_r$  and  $\phi$  in 3-D Space

and the maximum  $\phi$  may be defined as

$$\phi_{max} = 2 \cdot \pi - \sin^{-1}\left(\frac{1}{\sqrt{5}}\right) \approx 333.435^\circ \quad (3.30)$$

The minimum and maximum  $\phi$  are apparent in the contour plot of Figure 3.5. Notice that a 2x1 elliptical formation not only occurs in-plane, as shown by Sabol [20], but can also occur in a variety of out-of-plane formations.

### 3.5 Relative Quotient

The relationship between  $z_{max}$  and  $a_e$  was defined as the relative quotient in Eq.(3.24). The validity of this linear relationship may be shown by a typical plot of eccentricity versus  $a_e$  and  $z_{max}$  for a constant  $\phi$  as seen in Figure 3.6 or more clearly visible in its contour plot, Figure 3.7.



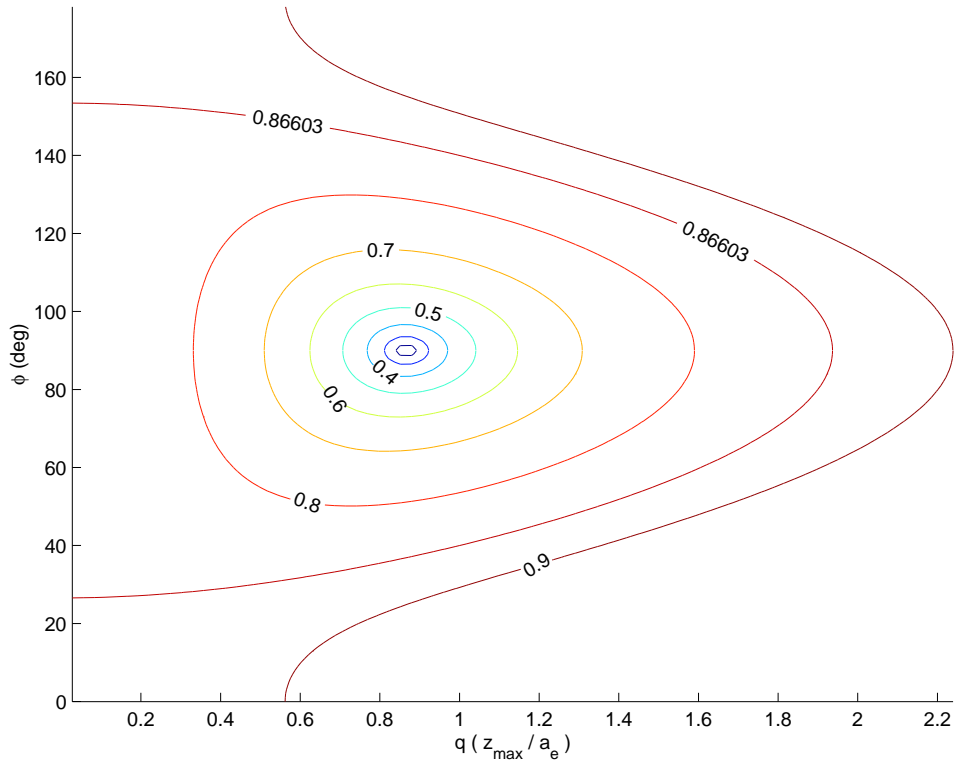


Figure 3.4 Contour Plot of  $q_r$  and  $\phi$  with Constant Lines of Eccentricity

### 3.6 Formation Angles

*3.6.1 Parametric to Physical.* As previously alluded to,  $\beta$  and  $\phi$  are parametric angles, not physical angles. A method similar to finding the true anomaly from the eccentric anomaly for a Keplerian orbit is used to find the relationship between the physical and parametric angles. Although, here both angles are measured from the center of the ellipse as seen in Figure 3.8. The deputy's elliptical path in the orbital plane is denoted below by the subscript “ $e$ ”.

$$4 \cdot x_e^2 + y_e^2 = a_e^2 \quad (3.31)$$

Conversely, the subscript “ $a$ ” denotes an auxiliary (circumscribed) circle with a radius of  $a_e$ .

$$x_a^2 + y_a^2 = a_e^2 \quad (3.32)$$

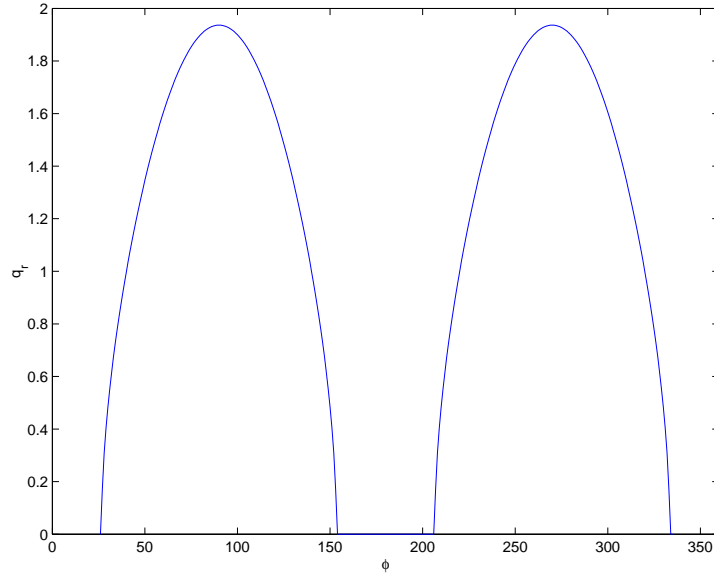


Figure 3.5 Example:  $\phi$  Versus  $q_r$  When Eccentricity Equals  $\frac{\sqrt{3}}{2}$

The physical  $\tilde{\beta}$  is related to an actual point on the formation by

$$\frac{y_e}{-x_e} = \tan(\tilde{\beta}) \quad (3.33)$$

whereas the parametric angle  $\beta$  is related to a point on the auxiliary circle by

$$\frac{y_a}{-x_a} = \tan(\beta) \quad (3.34)$$

The projection onto the auxiliary circle (see Figure 3.8) dictates that  $y_a = y_e$ .

Eqs.(3.33) and (3.34) are equated by solving each for  $y$ . The result is

$$-x_e \cdot \tan(\tilde{\beta}) = -x_a \cdot \tan(\beta) \quad (3.35)$$

Therefore, the relationship between parametric  $\beta$  and physical  $\tilde{\beta}$  is

$$\tan(\tilde{\beta}) = \frac{x_a}{x_e} \cdot \tan(\beta) \quad (3.36)$$

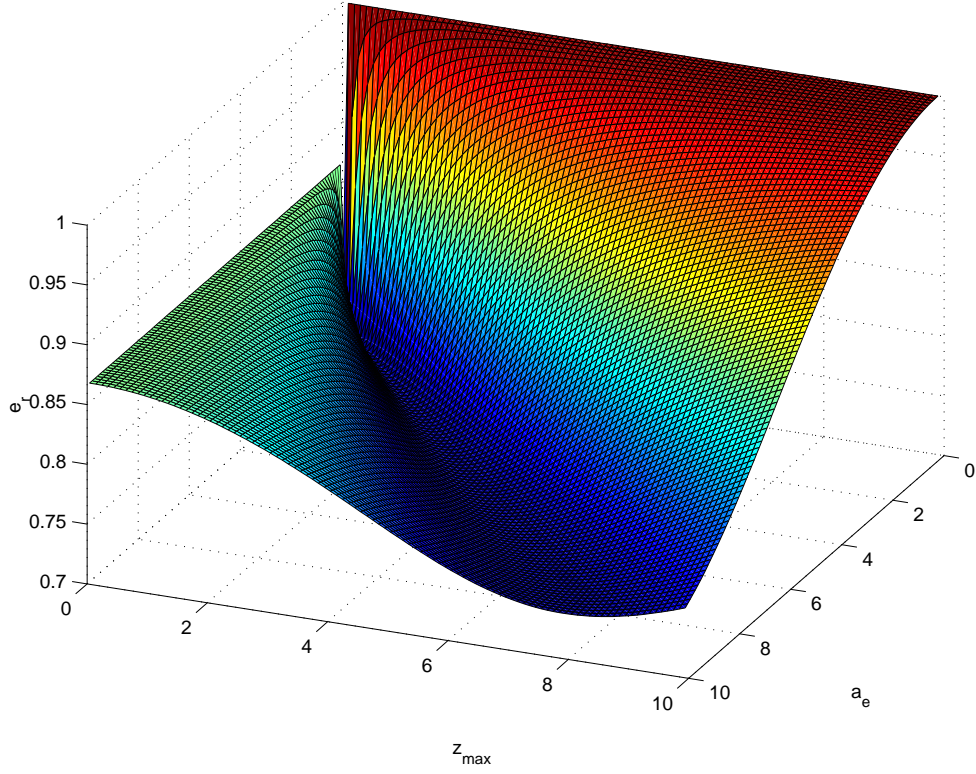


Figure 3.6  $e_r$  Versus  $a_e$  and  $z_{max}$  for  $\phi = 60^\circ$

Eqs.(3.31) and (3.32) are equated by solving each for  $y^2$ . The result is

$$a_e^2 - 4 \cdot x_e^2 = a_e^2 - x_a^2 \quad (3.37)$$

Manipulating Eq.(3.37) leads to

$$\frac{x_a}{x_e} = 2 \quad (3.38)$$

Therefore, the relationship of parametric  $\beta$  and physical  $\tilde{\beta}$  is expressed as

$$\tan(\tilde{\beta}) = 2 \cdot \tan(\beta) \quad (3.39)$$

Similar analysis is used to determine the same relationship between parametric  $\phi$  and physical  $\tilde{\phi}$ .

$$\tan(\tilde{\phi}) = 2 \cdot \tan(\phi) \quad (3.40)$$

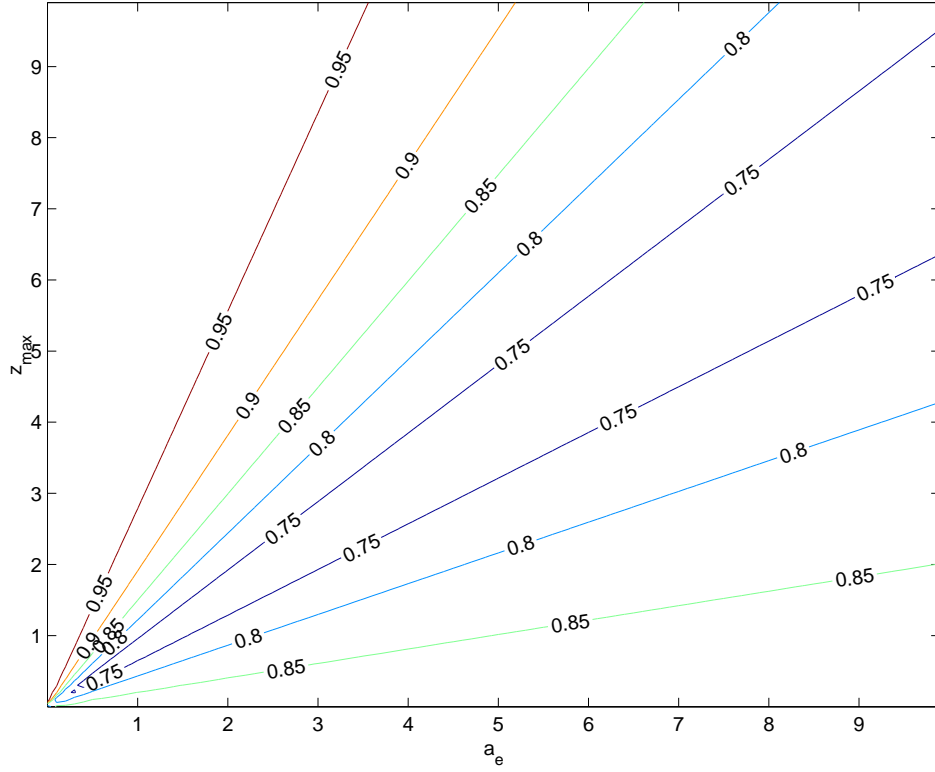


Figure 3.7  $a_e$  Versus  $z_{max}$  Contour Plot for Constant  $e_r$  at  $\phi = 60^\circ$

In addition, it is worth noting that differentiating Eq.(3.39) yields the in-plane angular velocity.

$$\dot{\beta} = \frac{2 \cdot \omega}{3 \cdot \sin(\beta)^2 + 1} \quad (3.41)$$

3.6.2 *Out-of-Plane Position.* When  $\beta = \phi$ , the relative position simplifies to

$$\vec{\Omega}_r = \begin{bmatrix} \frac{-a_e}{2} \cdot \cos(\phi) \\ a_e \cdot \sin(\phi) + y_d \\ 0 \end{bmatrix} \quad (3.42)$$

The vector  $\vec{\Omega}_r$  is referred to as the relative line of nodes because it represents the point where the satellite ascends through the reference orbital plane. From Eqs.(3.7)-(3.9)

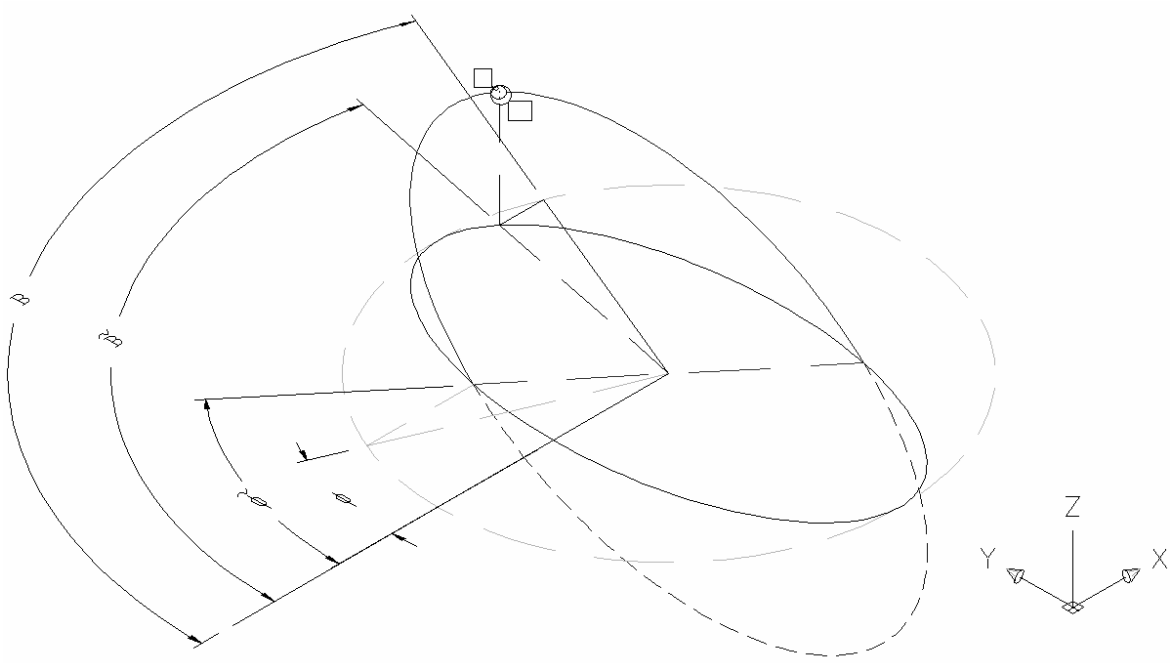


Figure 3.8 Physical Representation of  $\beta$ ,  $\tilde{\beta}$ ,  $\phi$  and  $\tilde{\phi}$

the relative position vector is expressed as

$$\vec{r}_r = \begin{bmatrix} \frac{-a_e}{2} \cdot \cos(\beta) \\ a_e \cdot \sin(\beta) + y_d \\ z_{\max} \cdot \sin(\beta - \phi) \end{bmatrix} \quad (3.43)$$

Therefore,

$$\vec{\Omega}_r \bullet \vec{r}_r = |\Omega_r| \cdot |r_r| \cdot \cos(\tilde{v}_r) \quad (3.44)$$

where  $\tilde{v}_r$  is the angle from the relative line of nodes to the position of the deputy in the relative plane, thereby termed relative argument of latitude. This angle seen in Figure 3.9 is

$$\tilde{v}_r = \cos^{-1} \left( \frac{(\cos(\beta) \cdot \cos(\phi) + 4 \cdot \sin(\phi) \cdot \sin(\beta))}{q_r \cdot \sqrt{1 + 3 \cdot \sin(\phi)^2} \cdot \sqrt{\kappa}} \right) \quad (3.45)$$

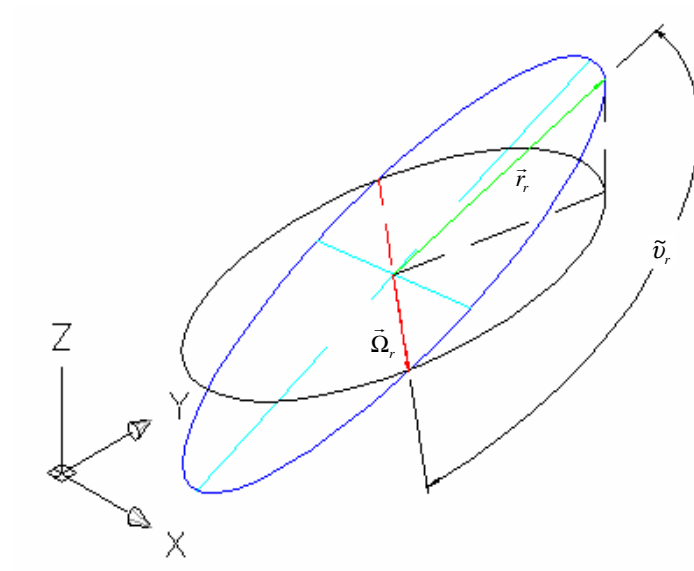


Figure 3.9 Relative Argument of Latitude

where

$$\kappa = q_r^2 + 4 \cdot \sin(\phi)^2 - 8 \cdot \sin(\phi) \cdot \cos(\beta) \cdot \cos(\phi) \cdot \sin(\beta) + (q_r^2 \cdot 3 - 8 \cdot \sin(\phi)^2 + 4) \cdot \sin(\beta)^2 \quad (3.46)$$

Figures 3.10 and 3.11 show a typical F<sup>3</sup>OS formation.

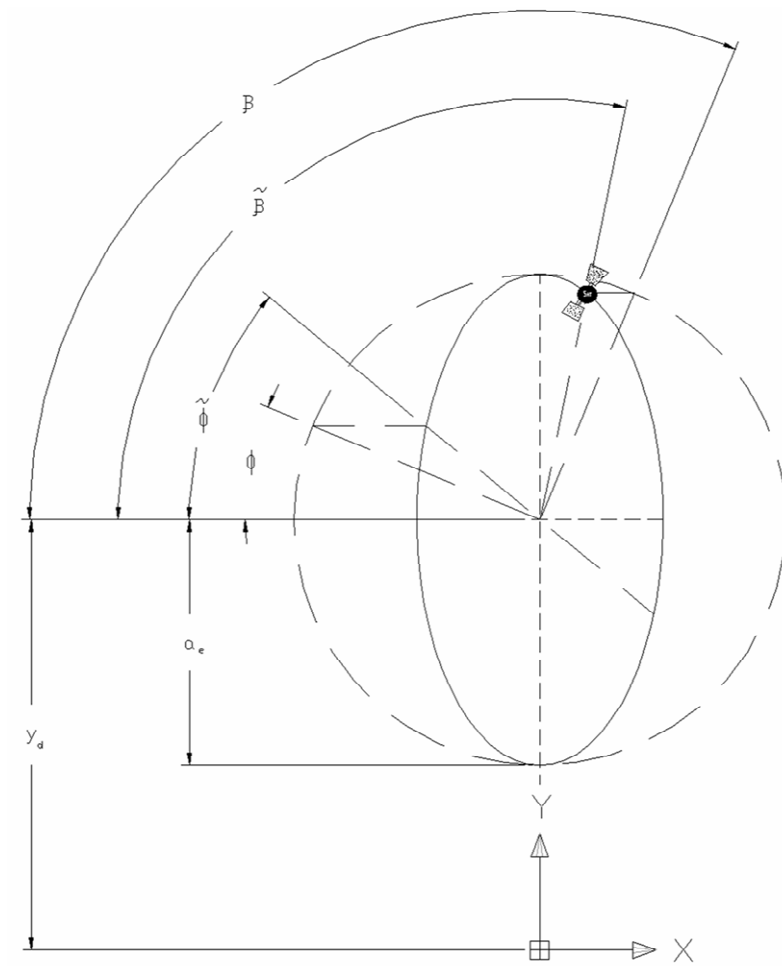


Figure 3.10 First-Order Force-Free Stationary Formations: In-Plane View





## IV. Mission Design

### 4.1 Preliminary Mission Design

*4.1.1 Mission Requirements.* The analysis begins by specifying a mission. An instantaneous time of observation, a ground target site, and the chief's orbital period specify the mission. The time of observation is defined by a GMST angle. The target site is specified by a latitude and longitude. Using the period

$$P = 2 \cdot \pi \cdot \sqrt{\frac{a^3}{\mu}} \quad (4.1)$$

where  $\mu$  is Kepler's constant, the radius of the chief is determined. It is worth noting that the period of the deputy satellites' (relative) motion equals the period of the chief's (absolute) orbital motion as given by Eq.(4.1).

*4.1.2 Satellite Requirements.* The purpose of the satellite requirements is to establish the chief's orbit. This is a basic point mass mission design problem covered in Wertz [27], but it is covered here to express the operational limitation and provide inputs for a numerical example. Assuming the chief is in a circular orbit, the chief's semi-major axis,  $a_c$ , coupled with the target site and look vector (specified by radar requirements) define the chief's instantaneous position vector. An established position vector limits the orbital plane. In particular, the inclination,  $i_c$ , is limited by the chief's latitude,  $L_c$ , similar to a launch-window problem. The inclination cannot be less than  $L_c$  for prograde orbits nor greater than  $180^\circ - L_c$  for retrograde orbits. The latitude of the chief, i.e., the angle the position vector makes with the equatorial plane, is given by

$$L_c = \frac{\pi}{2} - \cos^{-1} \left( \frac{\vec{r}_c \bullet \hat{K}}{a_c} \right) \quad (4.2)$$

Therefore, the inclination may only exist between  $\frac{\pi}{2} - \cos^{-1}(\vec{r}_c \bullet \hat{K}/a_c)$  and  $\frac{\pi}{2} + \cos^{-1}(\vec{r}_c \bullet \hat{K}/a_c)$ . Once the inclination is chosen, the right ascension of the ascending node,  $\Omega_c$ , is limited to two possible values by solving

$$\begin{bmatrix} \sin(\Omega_c) \cdot \sin(i_c) \\ -\cos(\Omega_c) \cdot \sin(i_c) \\ \cos(i_c) \end{bmatrix} \bullet \vec{r}_c = 0 \quad (4.3)$$

The argument of latitude,  $u_c$ , may then be solved using

$$\sin(u_c) = \frac{\vec{r}_c \bullet \hat{K}}{a_c \cdot \sin(i_c)} \quad (4.4)$$

Eqs.(4.1)-(4.4) yield  $a_c$ ,  $i_c$ ,  $\Omega_c$ , and  $u_c$  which are the only orbital elements needed to completely define the circular reference orbit.

An alternative is to first establish the orbital reference plane by selecting the inclination and right ascension of the ascending node, and then calculate the reference satellite's period.

*4.1.3 Radar Requirements.* Radar requirements include defining a look vector (chosen by an *az* and *el*), an imaging plane (chosen to be UV), and u-v points. With the target site and reference orbit specified, the main requirement driving the formation design is the spatial distribution of the satellites in the image plane, i.e., u-v points. The aim in selecting this particular input requirement is to provide a usable means of achieving a desired remote sensing performance (e.g. baseline distances for interferometry or moving target indication).

## 4.2 Perpendicular Constraint

In addition to specifying satellite location in the u-v plane, the first design approach will also require that the relative formation plane is perpendicular to the look

vector,  $\hat{L}$ . This eliminates the possibility of radar shadowing and may have additional benefits concerning the processing of the remote sensing data. This problem is a subset of the overall problem and is expressed as the perpendicular constraint. For multi-satellite arrays with the perpendicular constraint enforced, the satellites orbit in the same plane with respect to the chief but each loiters in a different stationary formation.

The angle between the unit normal of the formation plane and the unit look vector is given by

$$\theta_{error} = \cos^{-1}(\hat{L} \bullet \hat{n}_r) \quad (4.5)$$

According to Eq.(3.16),  $\hat{n}_r$  is a function of variables  $a_e$ ,  $z_{max}$ , and  $\phi$ , whereas  $\hat{L}$  is a function of inputs azimuth, elevation, latitude, GMST, longitude, semi-major axis of the chief, chief's inclination, chief's right ascension, and the chief's argument of latitude. For simplicity, we will only examine cases in which  $y_d = 0$ , that is, when the formation rotates about the chief. The perpendicular error can be expressed as

$$\cos(\theta_{error}) = \frac{2 \cdot \sin(\phi) \cdot L_r + \cos(\phi) \cdot L_s + \frac{-1}{q_r} \cdot L_w}{\sqrt{4 \cdot \sin(\phi)^2 + \cos(\phi)^2 + \frac{1}{q_r^2}} \cdot \sqrt{L_r^2 + L_s^2 + L_w^2}} \quad (4.6)$$

where the constants  $L_r$ ,  $L_s$ , and  $L_w$  are the RSW components of the look vector. Therefore, if  $\theta_{error}$  equals 0 or  $\pi$ , the formation is parallel to the imaging plane. Furthermore, the formation plane coincides with the imaging plane due to the assumption of  $y_d = 0$ , thereby avoiding a projection transformation. The perpendicular constraint is actually a constraint on two variables,  $q_r$  and  $\phi$ . Taking Eq.(4.6) and squaring both sides, multiplying through by  $q_r^2$ , and then subtracting the left side from both sides, we are able to put Eq.(4.6) into the form of

$$A \cdot q_r^2 + B \cdot q_r = C \quad (4.7)$$

where

$$\begin{aligned}
A &= (4 \cdot L_s^2 + 3L_w^2 - L_r^2) \cdot \cos(\phi) + 4 \cdot L_r \cdot L_s \cdot \sin(\phi) \cdot \cos(\phi) - 4 \cdot L_s^2 - 4 \cdot L_w^2 \\
B &= -4 \cdot L_r \cdot L_w \cdot \sin(\phi) - 2 \cdot L_s \cdot L_w \cdot \cos(\phi) \\
C &= L_r^2 + L_s^2
\end{aligned} \tag{4.8}$$

For  $q_r$  to be real, the quantity  $B^2 + 4 \cdot A \cdot C$  must be positive. By simplifying  $B^2 + 4 \cdot A \cdot C$ , we are able to obtain

$$[-16 \cdot L_s^2(L_r^2 + L_s^2 + L_w^2)] \cdot \left[ \left( \left( \frac{L_r}{2 \cdot L_s} \right)^2 - 1 \right) \cos(\phi)^2 + \left( \frac{L_r}{L_s} \right) \cdot \sin(\phi) \cdot \cos(\phi) + 1 \right] \tag{4.9}$$

This is a sinusoidal function with the maximum value always occurring at zero. Therefore, only one value of  $\phi$  exists in order for  $q_r$  to be real. The value occurs when  $\phi$  equals the phase shift, or in other words when  $B^2 + 4 \cdot A \cdot C = 0$ .

$$\left( \left( \frac{L_r}{2 \cdot L_s} \right)^2 - 1 \right) \cos(\phi)^2 + \left( \frac{L_r}{L_s} \right) \cdot \sin(\phi) \cdot \cos(\phi) + 1 = 0 \tag{4.10}$$

Through the use of Eq.(A.10) in Appendix (A),

$$\left( \frac{L_r}{2 \cdot L_s} \right)^2 \cdot (1 - \sin(\phi)^2) + \left( \frac{L_r}{L_s} \right) \cdot \sin(\phi) \cdot \cos(\phi) + \sin(\phi)^2 = 0 \tag{4.11}$$

The left of Eq.(4.11) is a perfect square and may be reduced to

$$\left( \frac{L_r}{2 \cdot L_s} \cdot \cos(\phi) + \sin(\phi) \right)^2 = 0 \tag{4.12}$$

in other words

$$\phi = \tan^{-1} \left( \frac{L_r}{2 \cdot L_s} \right) \tag{4.13}$$

Substituting this expression into Eq.(4.7) and solving for  $q_r$  using the quadratic formula, leads to

$$q_r = \frac{\sqrt{\frac{1}{4} \cdot (L_r)^2 + (L_s)^2}}{L_w} \quad (4.14)$$

Therefore, the perpendicular constraint is enforced with Eqs.(4.13) and (4.14). If the perpendicular constraint is enforced, then  $q_r$  and  $\phi$  are constants, and the relative eccentricity is determined.

Given a desired  $(u_i, v_i)$  point, the procedure that follows solves for  $a_e$ ,  $z_{max}$ , and  $\beta_o$  utilizing the perpendicular constraint. The point  $(u_i, v_i)$  is interposed into GLP components and then rotated and translated into the RSW frame.

$$\begin{bmatrix} x_i \\ y_i \\ z_i \\ \Xi \end{bmatrix} = {}^{RSW}R^{IJK} \cdot {}^{IJK}R^{SEZ} \cdot {}^{SEZ}R^{GLP} \cdot \begin{bmatrix} u_i \\ 0 \\ v_i \\ \Xi \end{bmatrix} \quad (4.15)$$

Since the origin of the GLP frame is on the chief, only rotations are necessary. The in-plane components of the rotated and translated GLP points,  $x_i$  and  $y_i$ , are evaluated by examining their quadrant. Eqs.(3.4), (3.33), (3.39) and (4.15) are used to determine  $\beta_o$ . This would simply be

$$\beta_o = \tan^{-1} \left( \frac{-y_i}{2 \cdot x_i} \right) - \omega \cdot t \quad (4.16)$$

The ellipse, Eq.(3.12), must be projected in the chief's orbital plane. Therefore  $a_e$  is found using the in-plane components of the rotated and translated GLP points by

$$a_e = \sqrt{4 \cdot x_i^2 + y_i^2} \quad (4.17)$$

Eqs.(3.24), (4.14), and (4.17) lead to

$$z_{max} = \frac{\sqrt{(4 \cdot x_i^2 + y_i^2) \cdot (\frac{1}{4} \cdot L_r^2 + L_s^2)}}{L_w} \quad (4.18)$$

Eqs.(4.13), (4.16), (4.17), and (4.18) represent a formation perpendicular to the line of sight whose deputy is seen as  $(u_i, v_i)$  at the time of observation.

### 4.3 Co-formation Constraint

It may be desirable to have all of the satellites in the same stationary formation. When the chief satellite possesses a repeating ground track and all of the satellites are confined in the same formation, the formation will reoccur with the same spatial distribution over the same ground target. For deputy satellites to exist in the same formation, each deputy must have  $a_e$ ,  $y_d$ ,  $z_{max}$ , and  $\phi$  in common. Enforcing the perpendicular constraint on satellites in the same formation severely limits the possibilities when looking for three or greater points (two or more deputies) on the imaging plane. To allow for more options, the perpendicular constraint is released. For three points on the imaging plane, an infinite number of solutions exist. The solution here minimizes the in-plane projection, i.e., minimizing  $a_e$ . A separate solution that yields four points on the imaging plane where the three deputies are in the same formation is an extension of the three point solution. Unfortunately, the solution requires a numerical solver. The three and four point methods make another subset of the overall problem and are termed as the co-formation constrained problem.

*4.3.1 Three Point Array (Minimizing  $a_e$ ).* In this section, six equations are developed, three for each of the two u-v points, where each u-v point represents a unique deputy, and the deputy satellites exist in the same formation. The solution to the six equations leads to a formation description whose  $a_e$  is minimal. The first equation constrains both deputy satellites to the same in-plane projected 2x1 ellipse.

The second equation constrains the  $i^{th}$  deputy satellites to a line of sight that passes through a given  $(u_i, v_i)$  point. The third equation equates the slope of the in-plane projected line of sight to the slope of the in-plane projected ellipse. To begin, the inputs  $(u_1, v_1)$  and  $(u_2, v_2)$  from the radar requirements are converted to the RSW coordinate system,

$$\begin{bmatrix} r_i \\ s_i \\ w_i \\ \Xi \end{bmatrix} = {}^{RSW}R^{IJK} \cdot {}^{IJK}R^{SEZ} \cdot {}^{SEZ}R^{GLP} \cdot \begin{bmatrix} u_i \\ 0 \\ v_i \\ \Xi \end{bmatrix} \quad (4.19)$$

where  $(r_i, s_i, w_i)$  represents the required projection point of the  $i^{th}$  satellite in the RSW frame. Note that here, contrary to the last section, the imaging plane does not coincide with the formation plane. For the three point case,  $i$  is 1 or 2. The first equation is the in-plane elliptical equation given by,

$$\frac{4 \cdot x_i^2}{a_e^2} + \frac{(y_i - y_d)^2}{a_e^2} = 1 \quad (4.20)$$

where  $(x_i, y_i, z_i)$  represents the position of the  $i^{th}$  satellite in the RSW frame. This equation assists in constraining the satellites to a unique formation. The second equation is a line in the RSW coordinates constraining the projection of the satellite's position to the given u-v point. The line of sight equation is formulated from the target site's position in the RSW coordinates  $(T_r, T_s, T_w)$  and the u-v projection points in the RSW coordinates by using a two-point line equation. The equation for the line of sight is

$$\frac{x_i - r_i}{T_r - r_i} = \frac{y_i - s_i}{T_s - s_i} = \frac{z_i - w_i}{T_w - w_i} \quad (4.21)$$

Eliminating the “z” term yields the projection of the line of sight in the reference orbital plane (R-S plane) and is given by

$$y_i - T_s = \left( \frac{r_i - T_r}{s_i - T_s} \right) \cdot (x_i - T_r) \quad (4.22)$$

This leads to the third equation which essentially minimizes the  $a_e$  parameter through tangent point assessment. That is, the lines of sight will intersect the elliptical cylinder at points of tangency as shown in Figure 4.1. The slope for a point along the projected ellipse, Eq.(4.20), is determined by implicit differentiation

$$\frac{\partial y_i}{\partial x_i} = \frac{4 \cdot x_i}{y_d - y_i} \quad (4.23)$$

and equated to the slope of the projected line of sight giving the third equation.

$$\frac{4 \cdot x_i}{y_d - y_i} = \frac{r_i - T_r}{s_i - T_s} \quad (4.24)$$

With  $i = 1$  and  $i = 2$ , Eqs.(4.20), (4.22), and (4.24) make six equations with six unknowns which are  $x_1$ ,  $y_1$ ,  $x_2$ ,  $y_2$ ,  $y_d$ , and  $a_e$ . The six unknowns are solved for analytically. The parameter which depicts the position of the satellite in the projected ellipse,  $\beta_o$ , is solved for each satellite using Eq.(4.16). The out-of-plane position in the RSW coordinates for the  $i^{th}$  satellite,  $z_i$ , is solved by substituting  $x_i$  and  $y_i$  into Eq.(4.21). Having the position of both satellites,  $(x_1, y_1, z_1)$  and  $(x_2, y_2, z_2)$ , the formation plane is defined as

$$C_a \cdot x + C_b \cdot y + C_c \cdot z + C_d = 0 \quad (4.25)$$



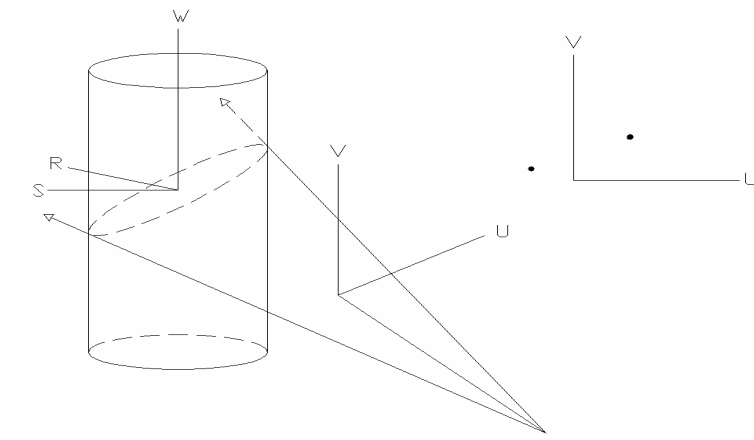


Figure 4.1 Two Tangent Site Vectors

where  $C_a$ ,  $C_b$ ,  $C_c$ , and  $C_d$  are found with the solved points  $(x_1, y_1, z_1)$ ,  $(x_2, y_2, z_2)$  and  $(0, y_d, 0)$ .

$$\begin{aligned}
 C_a &= y_1 \cdot z_2 - z_1 \cdot y_2 - y_d \cdot z_2 + y_d \cdot z_1 \\
 C_b &= x_2 \cdot z_1 - x_1 \cdot z_2 \\
 C_c &= (x_2 - x_1) \cdot y_d + x_1 \cdot y_2 - x_2 \cdot y_1 \\
 C_d &= (x_1 \cdot z_2 - x_2 \cdot z_1) \cdot y_d
 \end{aligned} \tag{4.26}$$

The point  $(0, y_d, 0)$  is the point which the formation rotates about, termed the pseudo-chief, which for F<sup>3</sup>OS formations is a point offset of the chief in the velocity direction. The intersection of this plane and the cylinder created by Eq.(4.20) provide  $z_{max}$  and  $\phi$ .

$$\phi = \tan^{-1} \left( \frac{C_a}{2 \cdot C_b} \right) \tag{4.27}$$

$$z_{\max} = \frac{a_e}{C_c} \cdot \sqrt{\frac{C_a^2}{4} + C_b^2} \tag{4.28}$$

Through examination, the normal of the plane is  $C_a \cdot \hat{R} + C_b \cdot \hat{S} + C_c \cdot \hat{W}$ , which demonstrates that Eqs.(4.27) and (4.28) have the same form as Eqs.(4.13) and (4.14) of the perpendicular constraint.

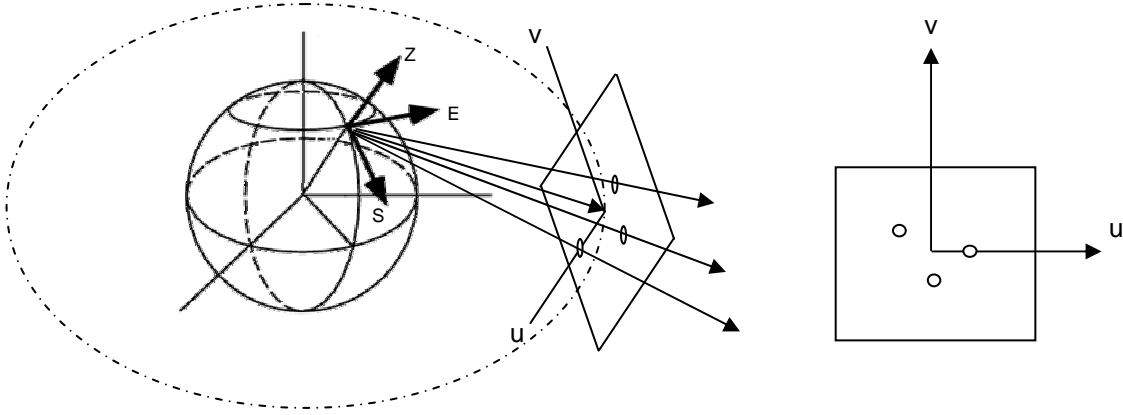


Figure 4.2 Three Line of Sight Vectors

*4.3.2 Four Point Array.* This section extends the problem to four points, i.e., three deputies. The initial calculations are similar to the initial equations of the three point solution with the exception of having a third deputy. The line of sight vectors are calculated from Eq.(4.21) (see Figure 4.2). Eq.(4.20) represents the projected formation but may be thought of as a cylinder in three-dimensional space. The intersection of each line in Eq.(4.21) and the elliptical cylinder, Eq.(4.20), has the solution of a single point in space, two points in space, or no solution (see Figure 4.3). Each intersection point (discriminated by  $k$ ) is a function of the semi-major axis of the elliptical cylinder,  $a_e$ , and the center of the elliptical cylinder determined by  $y_d$ . Each intersection point represents a potential deputy position with the restraint that the intersection(s) of the first line represent the position of the first deputy,  $(x_1^k, y_1^k, z_1^k)$ , the intersection(s) of the second line represent the position of the second deputy,  $(x_2^k, y_2^k, z_2^k)$ , and the intersection(s) of the third line represent the position of the third deputy,  $(x_3^k, y_3^k, z_3^k)$ . One intersection from each line, for a total of three intersection points, leads to one set of solutions. Since there is a possibility of having two intersection points ( $k = 1$  and  $k = 2$ ) per line, there are eight potential sets of solutions. For each set of three intersection points to be a viable solution, the intersection points and the pseudo-chief must lie in the same plane, the relative formation plane. To determine if the three points lie in the

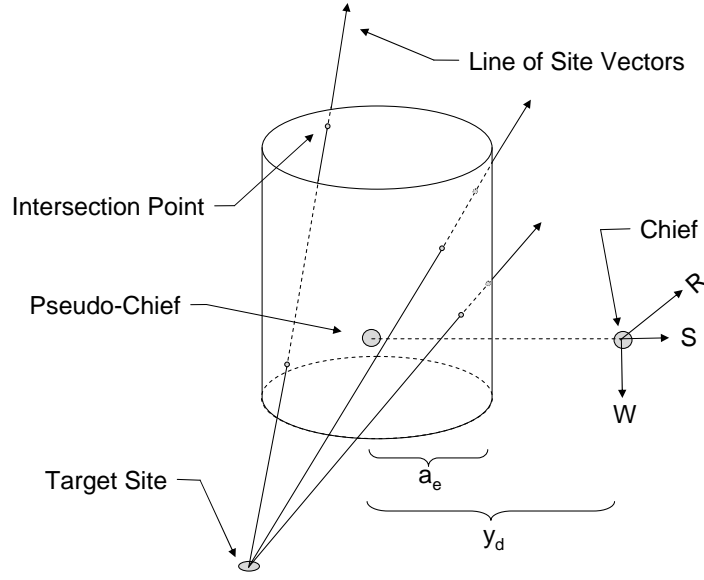


Figure 4.3 Line of Sight Vectors Intersecting a Projection Cylinder

same plane as the pseudo-chief, vectors are created beginning at the pseudo-chief and extending to each intersection point (see Figure 4.4). The three vectors created may be thought of as three edge vectors used to determine a parallelepiped. The volume of a parallelepiped is the absolute value of the scalar triple product of the three edge vectors. If the edge vectors of the parallelepiped lie in the same plane, then the volume is zero, resulting in a value of zero for the scalar triple product. Therefore, the three intersection points and the pseudo-chief lie in the same plane if they satisfy

$$\begin{pmatrix} x_1^k \\ y_1^k - y_d \\ z_1^k \end{pmatrix} \cdot \left[ \begin{pmatrix} x_2^k \\ y_2^k - y_d \\ z_2^k \end{pmatrix} \times \begin{pmatrix} x_3^k \\ y_3^k - y_d \\ z_3^k \end{pmatrix} \right] = 0 \quad (4.29)$$

This provides multiple  $a_e$  and  $y_d$  combinations for each set of three intersection points. With the intersection point  $(x_i^k, y_i^k, z_i^k)$  representing the position of the  $i^{th}$  satellite and knowing that all of the satellites lie in the same plane,  $\beta_o$  is solved for by substituting the appropriate  $x_i$  and  $y_i$  into Eq.(4.16) which requires a quadrant

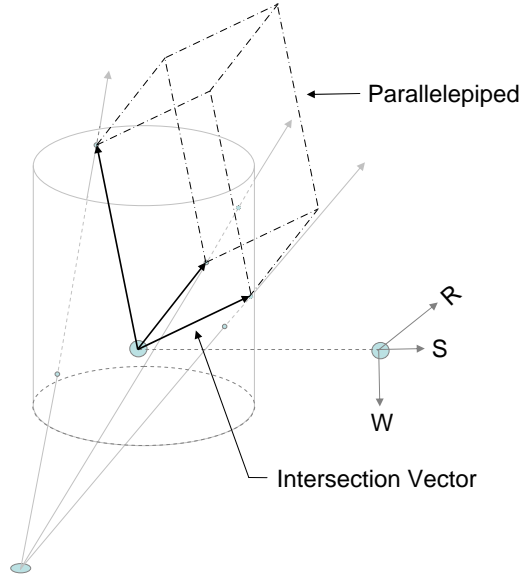


Figure 4.4 Parallelepiped and Intersection Vectors

check. Using any two of the three intersection points,  $\phi$  is determined from Eq.(4.27) where once again a quadrant check is necessary, and  $z_{max}$  is obtained from Eq.(4.28).

#### 4.4 Numerical Examples

*4.4.1 Perpendicular.* We are interested in viewing Damascus, Syria at a latitude of  $35^\circ$  North and longitude of  $38^\circ$  East. Due to restriction of the target site, the ideal azimuth and elevation are given as  $20^\circ$  and  $50^\circ$  respectively. The reference satellite has a radius of 7000 km, and this puts the range at nearly 787.84 km. A favorable look vector may be achieved by the reference satellite being in an inclination of  $87^\circ$  with a right ascension of  $37.4^\circ$  and having an argument of latitude of  $38.95^\circ$ . Figure 4.5 illustrates the reference orbit, target site, and look vector.

Specifying u-v points of (-100,300) meters and (100,100) meters, the perpendicular constraint equation yields  $\phi = 35.924^\circ$  and  $q_r = 3.979$ . This places the first deputy in a formation of  $a_e = 405.6$  meters and  $z_{max} = 1614.1$  meters at  $\beta_o = 66.5^\circ$ . The second deputy satellite is in a formation with  $a_e = 158.7$  meters and  $z_{max} = 631.5$

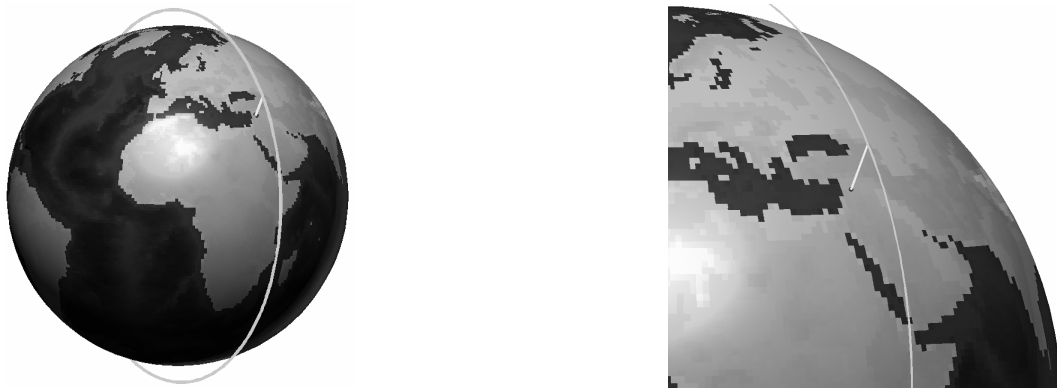


Figure 4.5 Perpendicular Constraint Example: Representation of The Reference Orbit, Target Site, and Look Vector

meters and located at  $\beta_o=74.7^\circ$ . Figures 4.6 and 4.7 illustrate the formation in the RSW and UV coordinate frames respectively.

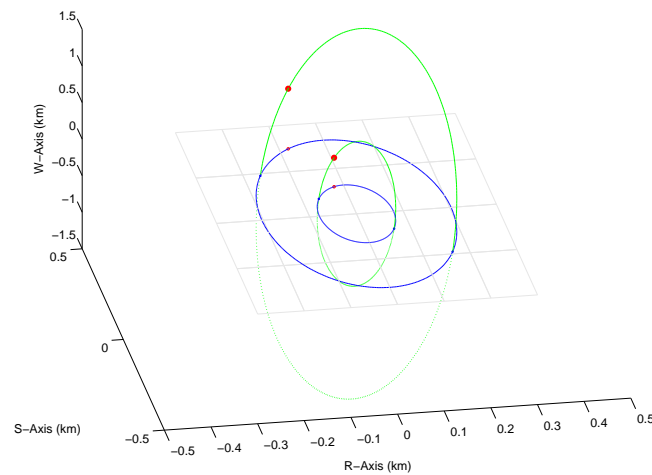


Figure 4.6 Perpendicular Constraint Example: Formation Plot with Satellites in RSW

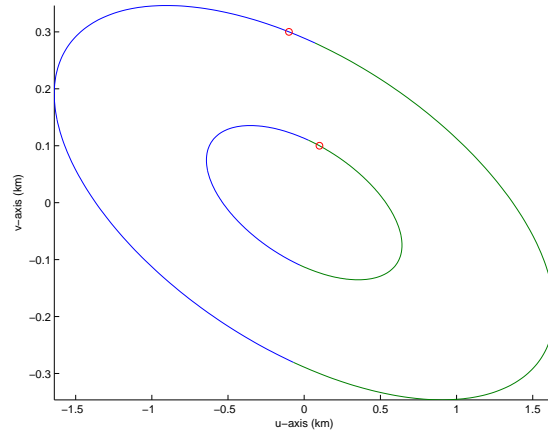


Figure 4.7 Perpendicular Constraint Example: Formation Plot with Satellites in UV

4.4.2 *Minimizing  $a_e$ .* We are interested in viewing Kabul, Afghanistan at a latitude of  $34^\circ$  North and longitude of  $69^\circ$  East. Due to restriction of the target site, the ideal azimuth and elevation are given as  $170^\circ$  and  $4^\circ$  respectively. The reference satellite has a radius of 7000 km, and this puts the range at nearly 2473.5 km. A favorable look vector may be achieved by the reference satellite being in an inclination of  $20^\circ$  with a right ascension of  $30.87^\circ$  and having an argument of latitude of  $43.51^\circ$ . Figure (4.8) shows the reference orbit with respect to the look vector and target site.

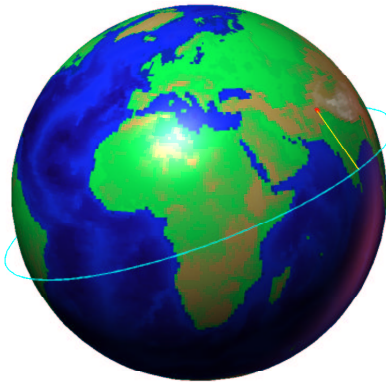


Figure 4.8 Minimum  $a_e$  Example: Representation of The Reference Orbit, Target Site, and Look Vector

Specifying symmetric u-v points of (150,150) meters and (-150,-150) meters, the co-formation (minimizing  $a_e$ ) yields an  $a_e$  of 109.1 meters, a  $z_{max}$  of 951.6 meters, and  $y_d$  is nearly zero. The  $\phi$  parameter is equal to  $120.84^\circ$ . The deputies have a  $\beta_o$  of  $88.29^\circ$  and  $271.7^\circ$ . Figures 4.9 and 4.10 demonstrates the resulting formation in the RSW and UV coordinate frame.

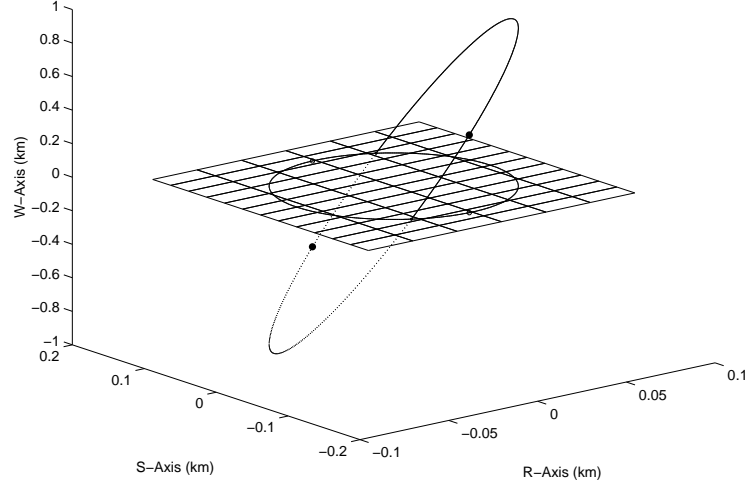


Figure 4.9 Minimum  $a_e$  Example: Formation Plot with Satellites in RSW

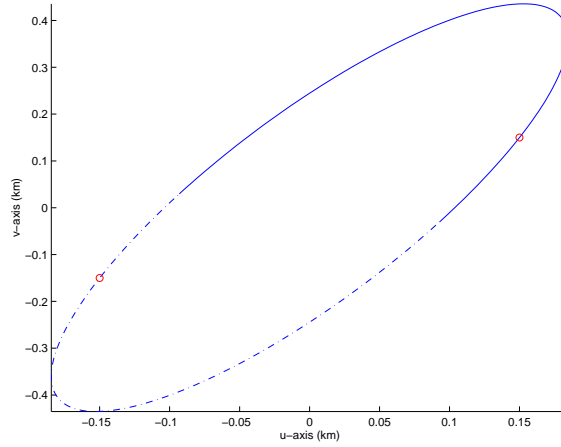


Figure 4.10 Minimum  $a_e$  Example: Formation Plot with Satellites in UV

*4.4.3 Three Deputy Array.* The United States has a particular interest in looking at Tbilisi, the capital city of the Republic of Georgia, at noon UTC on the 7th of July 2005. Tbilisi is located at  $45^\circ$  N latitude and  $40^\circ$  E longitude. The current

space asset's reference satellite orbits in the equatorial plane and has a period of 1 hour and 37 minutes. It will be directly South of the city and  $2^\circ$  off of the horizon at the time of interest. The question is what configuration, i.e., formation parameter must it be in to have a 30 meter equilateral spatial distribution of  $(0,17.32)$ ,  $(-15,-8.66)$ , and  $(15,-8.66)$ . Figure 4.11 shows all of the possibilities for  $a_e$  between 15 meters and 50 meters. The  $a_e$  chosen is 50 meters, letting  $y_d$  be 4.92 meters ahead

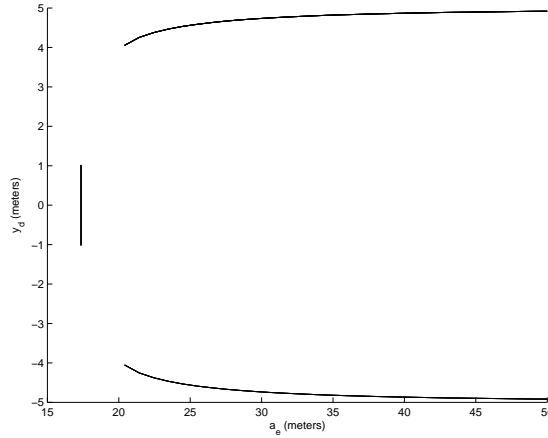


Figure 4.11 Three Deputy Example: Possible  $a_e$ ,  $y_d$  Values

or behind the chief in the velocity direction. Figure 4.12 is a plot of the deputies in the RSW frame, and Figure 4.13 reveals the UV plot when  $y_d$  is a positive 4.92 meters.

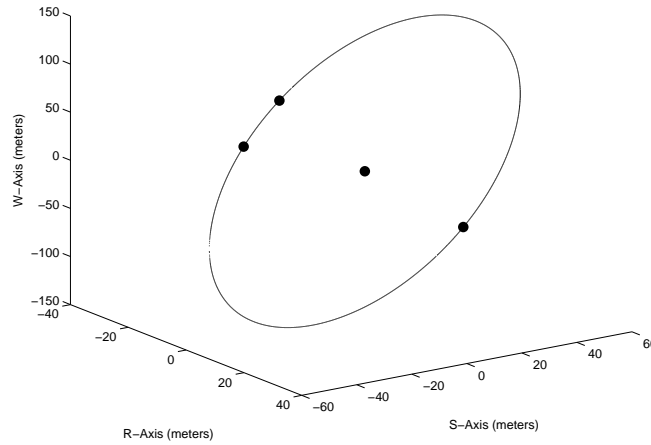


Figure 4.12 Three Deputy Example: Formation Plot with Satellites in RSW



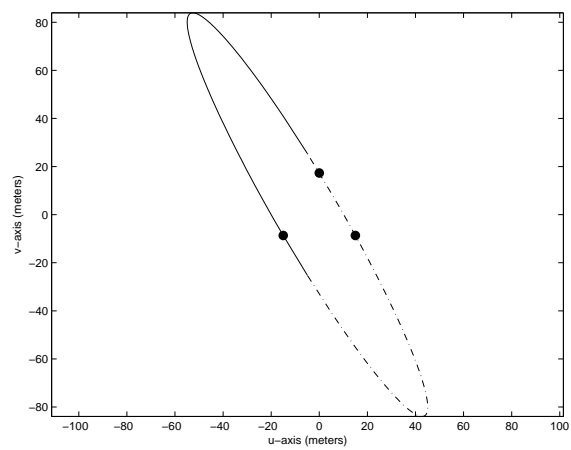


Figure 4.13 Three Deputy Example: Formation Plot with Satellites in UV

## *V. Conclusions and Recommendations*

### *5.1 Conclusions*

The algorithms developed in this work correlate the instantaneous geometric requirements of remote sensing to the dynamics of force-free first-order stationary satellite formations. Given a set of requirements, the algorithms constitute a relatively quick systematic way to calculate formation conditions that yield a feasible satellite distribution in an imaging plane relative to a chosen target site on the ground. Furthermore, these algorithms assist to bridge the gap that divides remote sensing requirements and satellite orbital parameters.

### *5.2 Recommendations*

The ideas presented are readily expandable to optimization routines or feasibility studies that evaluate multiple target sites, assess reconfiguration maneuvers, utilize perpendicular formation error, employ drifting formations, or even examine continuous observation times.

As alluded to above, there are several possible areas of further exploration. They include expanding the u-v distribution correlations to include drifting formations or validating the algorithms through an external source such as STK, Satellite Tool Kit. Although the limitations of Hill's equations are known, the limitations of the equations and algorithms derived here could be further explored and quantified. Although it has not been explicitly stated, the author has performed time duration analysis to specify the u-v points over a period of time. This area has great potential for future research. Another idea that has potential and was briefly examined incorporates a minimization routine with spacial distributions at multiple target sites to reduce reconfiguration costs.

The use of multiple apertures in space for remote sensing purposes is a topic of great military interest. The topic is highly interdisciplinary, requiring expertise from

several different technical fields. It is hoped that this work will provide the initial tools necessary for researchers in these fields to begin communicating in a way that will lead to innovative solutions to the problems associated with this topic.

## Appendix A. Trigonometric Relations

$$\cos(\theta) = \cos(-\theta) = \sin\left(\frac{\pi}{2} - \theta\right) \quad (\text{A.1})$$

$$\sin(\theta) = -\sin(-\theta) = \cos\left(\frac{\pi}{2} - \theta\right) \quad (\text{A.2})$$

$$\tan(\theta) = -\tan(-\theta) = \cot\left(\frac{\pi}{2} - \theta\right) \quad (\text{A.3})$$

$$\sin 2 \cdot \theta = 2 \cdot \cos \theta \sin \theta \quad (\text{A.4})$$

$$\cos 2 \cdot \theta = \cos^2 \theta - \sin^2 \theta = 2 \cdot \cos^2 \theta - 1 = 1 - 2 \sin^2 \theta \quad (\text{A.5})$$

$$\tan 2 \cdot \theta = 2 \cdot \tan \theta / (1 - \tan^2 \theta) \quad (\text{A.6})$$

$$\sin \frac{\theta}{2} = \pm \sqrt{\frac{(1 - \cos \theta)}{2}} \quad (\text{A.7})$$

$$\cos \frac{\theta}{2} = \pm \sqrt{\frac{(1 + \cos \theta)}{2}} \quad (\text{A.8})$$

$$\tan \frac{\theta}{2} = \frac{\sin \theta}{(1 + \cos \theta)} \quad (\text{A.9})$$

$$\cos^2 \theta + \sin^2 \theta = 1 \quad (\text{A.10})$$

$$\sec^2 \theta - \tan^2 \theta = 1 \quad (\text{A.11})$$

$$\cos^2 \theta - \cot^2 \theta = 1 \quad (\text{A.12})$$

$$\sin^2 \theta = \frac{1}{2} (1 - \cos 2 \cdot \theta) \quad (\text{A.13})$$

$$\cos^2 \theta = \frac{1}{2} (1 + \cos 2 \cdot \theta) \quad (\text{A.14})$$

$$\tan^2 \theta = \frac{(1 - \cos 2 \cdot \theta)}{(1 + \cos 2 \cdot \theta)} \quad (\text{A.15})$$

$$\sin(A + B) = \sin A \cos B + \cos A \sin B \quad (\text{A.16})$$

$$\sin(A - B) = \sin A \cos B - \cos A \sin B \quad (\text{A.17})$$

$$\cos(A + B) = \cos A \cos B - \sin A \sin B \quad (\text{A.18})$$

$$\cos(A - B) = \cos A \cos B + \sin A \sin B \quad (\text{A.19})$$

$$\tan(A + B) = \frac{(\tan A + \tan B)}{(1 - \tan A \tan B)} \quad (\text{A.20})$$

$$\tan(A - B) = \frac{(\tan A - \tan B)}{(1 + \tan A \tan B)} \quad (\text{A.21})$$

$$\sin A + \sin B = 2 \cdot \sin \frac{1}{2}(A + B) \cos \frac{1}{2}(A - B) \quad (\text{A.22})$$

$$\sin A - \sin B = 2 \cdot \cos \frac{1}{2}(A + B) \sin \frac{1}{2}(A - B) \quad (\text{A.23})$$

$$\cos A + \cos B = 2 \cdot \cos \frac{1}{2}(A + B) \cos \frac{1}{2}(A - B) \quad (\text{A.24})$$

$$\cos A - \cos B = -2 \cdot \sin \frac{1}{2}(A + B) \sin \frac{1}{2}(A - B) \quad (\text{A.25})$$

$$\tan A + \tan B = \sin \frac{(A + B)}{(\cos A \cos B)} \quad (\text{A.26})$$

$$\tan A - \tan B = \sin \frac{(A - B)}{(\cos A \cos B)} \quad (\text{A.27})$$

$$\sin^2 A + \sin^2 B = 1 - \cos(A + B) \cos(A - B) \quad (\text{A.28})$$

$$\sin^2 A - \sin^2 B = \sin(A + B) \sin(A - B) \quad (\text{A.29})$$

$$\cos^2 A + \sin^2 B = 1 - \sin(A + B) \sin(A - B) \quad (\text{A.30})$$

$$\cos^2 A - \sin^2 B = \cos(A + B) \cos(A - B) \quad (\text{A.31})$$

$$\cos^2 A + \cos^2 B = 1 + \cos(A + B) \cos(A - B) \quad (\text{A.32})$$

$$\cos^2 A - \cos^2 B = -\sin(A + B) \sin(A - B) \quad (\text{A.33})$$

## *Appendix B. MATLAB<sup>®</sup> One Axis Rotation Code*

The following MATLAB<sup>®</sup> m-file is used to create a rotation matrix that rotates the one axis through “degrees”.

```
%Axis One Rotation Matrix
function M = ROT1(degrees);
M = [1  0          0          0;
      0  cos(degrees) sin(degrees) 0;
      0 -sin(degrees) cos(degrees) 0;
      0  0          0          1];
%Matthew Press, 2003
```

### *Appendix C. MATLAB<sup>®</sup> Two Axis Rotation Code*

The following MATLAB<sup>®</sup> m-file is used to create a rotation matrix that rotates the two axis through “degrees”.

```
%Axis Two Rotation Matrix
function M = ROT2(degrees);
M = [cos(degrees) 0 -sin(degrees) 0;
      0           1  0           0;
      sin(degrees) 0  cos(degrees) 0;
      0           0  0           1];
%Matthew Press, 2003
```

### *Appendix D. MATLAB<sup>®</sup> Three Axis Rotation Code*

The following MATLAB<sup>®</sup> m-file is used to create a rotation matrix that rotates the three axis through “degrees”.

```
%Axis Three Rotation Matrix
function M = ROT3(degrees);
M = [cos(degrees) sin(degrees) 0 0;
     -sin(degrees) cos(degrees) 0 0;
      0      0      1 0;
      0      0      0 1];
%Matthew Press, 2003
```



## *Appendix E. MATLAB<sup>®</sup> GLP to SEZ*

The following MATLAB<sup>®</sup> m-file is used to rotate GLP coordinates to SEZ coordinates.

```
% GLP to SEZ
function [S,E,Z]= GLP2SEZ(G,L,P,az,el,rho);

for k = 1:max(size(G));
    SEZ = ROT3(az-pi/2)*ROT1(-el)*...
    [1 0 0 0;0 1 0 rho;0 0 1 0;0 0 0 1]*[G(k);L(k);P(k);1];
    S(k) = SEZ(1);
    E(k) = SEZ(2);
    Z(k) = SEZ(3);
end
%Matthew Press, 2003
```

## *Appendix F. MATLAB<sup>®</sup> SEZ to IJK*

The following MATLAB<sup>®</sup> m-file is used to rotate SEZ coordinates to IJK coordinates.

```
%SEZ to IJK
function [I,J,K] = SEZ2IJK(S,E,Z,L,l,re);

for k = 1:max(size(S));
    IJK = ROT3(-1)*ROT2(L-(pi/2))*...
    [1 0 0 0;0 1 0 0;0 0 1 re;0 0 0 1]*[S(k);E(k);Z(k);1];
    I(k) = IJK(1);
    J(k) = IJK(2);
    K(k) = IJK(3);
end

%Matthew Press, 2003
```

## *Appendix G. MATLAB<sup>®</sup> IJK to RSW*

The following MATLAB<sup>®</sup> m-file is used to rotate IJK coordinates to RSW coordinates.

```
% IJK to RSW
function [R,S,W] = IJK2RSW(I,J,K,a,In,Om,u);

for k = 1:max(size(I));
    RSW = [1 0 0 -a;0 1 0 0;0 0 1 0;0 0 0 1]*...
    ROT3(u)*ROT1(In)*ROT3(Om)*[I(k);J(k);K(k);1];
    R(k) = RSW(1);
    S(k) = RSW(2);
    W(k) = RSW(3);
end
%Matthew Press, 2003
```

## *Appendix H. MATLAB<sup>®</sup> RSW to IJK*

The following MATLAB<sup>®</sup> m-file is used to rotate RSW coordinates to IJK coordinates.

```
%RSW to IJK
function [I,J,K] = RSW2IJK(R,S,W,a,In,Om,u);

for k = 1:max(size(R));
    IJK = ROT3(-Om)*ROT1(-In)*ROT3(-u)*...
    [1 0 0 a;0 1 0 0;0 0 1 0;0 0 0 1]*[R(k);S(k);W(k);1];
    I(k) = IJK(1);
    J(k) = IJK(2);
    K(k) = IJK(3);
end

%Matthew Press, 2003
```

## *Appendix I. MATLAB<sup>®</sup> IJK to SEZ*

The following MATLAB<sup>®</sup> m-file is used to rotate IJK coordinates to SEZ coordinates.

```
%IJK to SEZ
function [S,E,Z] = IJK2SEZ(I,J,K,L,l,re);

for k = 1:max(size(I));

    SEZ = [1 0 0 0;0 1 0 0;0 0 1 -re;0 0 0 1]*...
    ROT2(-L+(pi/2))*ROT3(l)*[I(k);J(k);K(k);1];
    S(k) = SEZ(1);
    E(k) = SEZ(2);
    Z(k) = SEZ(3);
end

%Matthew Press, 2003
```

## *Appendix J. MATLAB<sup>®</sup> SEZ to GLP*

The following MATLAB<sup>®</sup> m-file is used to rotate SEZ coordinates to GLP coordinates.

```
%SEZ to GLP
function [G,L,P]= SEZ2GLP(S,E,Z,az,el,rho);

for k = 1:max(size(S));
    GLP = [1 0 0 0;0 1 0 -rho;0 0 1 0;0 0 0 1]*...
    ROT1(el)*ROT3(-az+pi/2)*[S(k);E(k);Z(k);1];
    G(k) = GLP(1);
    L(k) = GLP(2);
    P(k) = GLP(3);
end

%Matthew Press, 2003
```

### *Appendix K. MATLAB<sup>®</sup> GLP to UV*

The following MATLAB<sup>®</sup> m-file is used to rotate GLP coordinates to UV coordinates.

```
%GLP to UV
function [U,V]= GLP2UV(G,L,P,rho);
    for k = 1:max(size(G));
        U(k) = (rho/(L(k)+rho))*G(k);
        V(k) = (rho/(L(k)+rho))*P(k);
    end
%Matthew Press, 2003
```

## Bibliography

1. Bordner, Ralph E. III. *Estimation of Relative Satellite Formation Element Positions in Near Circular Orbits*. MS thesis, Air Force Institute of Technology, Wright-Patterson AFB OH, March 2001.
2. Buckingham, E. "On physically similar systems; Illustrations of the use of dimensional equations," *Phys.Rev.* (1914).
3. Clohessy, W. H. and R. S. Wiltshire. "Terminal Guidance System for Satellite Rendezvous," *Journal of the Aerospace Sciences*, 27:653–674 (1960).
4. Cornwell, T.J. *Imaging at Radio Wavelengths*. ESA SP-273, June 1987.
5. Das, Alok, et al. "TECHSAT 21: A Revolutionary Concept in Distributed Space Based Sensing," *Proceedings for the Guidance, Navigation and Control Conference, American Institute of Aeronautics and Astronautics*(Paper no. AIAA-98-5255):1–6 (August 1998).
6. DeCou, Anthony B. "Orbital Station-Keeping for Multiple Spacecraft Interferometry," *The Journal of the Astronautical Sciences*, 39(3):283–297 (July-September 1991).
7. Floria, L. *On the Definition of the Delaunay Similar Canonical Variables of Scheifele*. Mechanics Research Communications 21, 1994.
8. Gray, A. *Ruled Surfaces*. FL: CRC Press: Boca Raton, 1993.
9. Hilbert, D. and S. Cohn-Vossen. *Geometry and the Imagination*. New York: Chelsea.
10. Hill, G. W. "Researches in the Lunar Theory," *American Journal of Mathematics*, 1(1):5–26 (1878).
11. Irvin, David J. Jr. *A Study of Linear vs. Nonlinear Control Techniques for the Re-configuration of Satellite Formations*. MS thesis, Air Force Institute of Technology, Wright-Patterson AFB OH, March 2001.
12. Johnston, M. Daniel and Kerry T. Nock. *Free Flyer Optical Interferometry Trajectory Analysis*. Technologies for Optical Interferometry in Space, September 1991.
13. Kong, Edmund M., et al. "Optimal Trajectories and Orbit Design for Separated Spacecraft Interferometry," *NASA Langley Research Center: Massachusetts Institute of Technology*, (Contract No. 96-01) (November 1998).
14. Lovell, T. A. and S.G. Tragesser. *Analysis of the Reconfiguration and Maintenance of Close Spacecraft Formations*. 13th AAS/AIAA Space Flight Mechanics Meeting Paper No. AAS 03-139, Feb. 2003.



15. Lovell, Tragesser and Tollefson. "A Practical Guidance Methodology for Relative Motion of LEO Spacecraft Based on the Clohessy-Wiltshire Equations," *AAS/AIAA Space Flight Mechanics Meeting*, (AAS Paper 04-252) (Feb 8-12 2004).
16. Lovell, Horneman, Tragesser and Tollefson. "A Guidance Algorithm for Formation Reconfiguration and Maintenance Based on the Perturbed Clohessy-Wiltshire Equations," *AAS/AIAA Astrodynamics Specialist Conference*, (AAS Paper 03-649) (Aug 3-7 2003).
17. M. Guelman, M. Aleshin. "Optimal Bound Low Thrust Rendezvous With Fixed Terminal Approach Direction," *Technion-Israel Institute of Technology, Israel*, (AAS 97-648) (1997).
18. Meirovitch, Leonard. *Methods of Analytical Dynamics*. New York: McGraw-Hill Book Company, 1970.
19. Parker, T. W., et al. "Advanced Metrics for Optimizing Satellite Formations Performing Interferometry Missions." *Proceedings of AIAA/AAS Astrodynamics Specialist Conference*. Monterey, California: AIAA, 2002.
20. Sabol, C., Burns R. and C.A. McLaughlin. *Satellite Formation Flying Design and Evolution*. AAS/AIAA Space Flight Mechanics Meeting Paper No. AAS 99-121, Feb. 1999.
21. Schaub, Hanspeter and Kyle T. Alfriend. "J2 Invariant Relative Orbits for Spacecraft Formations," *NASA Flight Mechanics Symposium* (1999).
22. Schweighart, S. and R. Sedwick. *A Perturbative Analysis of Geopotential Disturbances for Satellite Cluster Formation Flying*. IEEE Aerospace Conference p. 1001 - 1019, Mar 2001.
23. Sedwick, R. J., et al. "Exploiting Orbital Dynamics and Micropropulsion for Aperture Synthesis Using Distributed Satellite Systems: Applications to Tech-Sat 21," *Defense and Civil Space Programs Conference and Exhibit*, (AIAA-98-5289):28-30 (October 1998).
24. Sedwick, R. J., et al. "Mitigation of Differential Perturbations in Formation Flying Satellite Clusters," *The Journal of the Astronautical Sciences*, 47(3 and 4):309-331 (July-December 1999).
25. Space Vehicles Directorate, AFRL. "Space Missions Using Satellite Clusters," <http://www.vs.afrl.af.mil/TechProgs/TechSat21/NGSC.html> (2001).
26. Vallado, D. A. *Fundamentals of Astrodynamics and Applications*. The McGraw-Hill Companies, Inc., 1997.
27. Wertz, James R. and Wiley J. Larson. *Space Mission Analysis and Design, Third Edition*. Microcosm Press, 1999.

28. Wiesel, William E. *Spaceflight Dynamics*. New York: McGraw-Hill, Inc., 1989.
29. Wiesel, William E. "Optimal Impulsive Control of Relative Satellite Motion," *submitted to Journal of Guidance, Control, and Dynamics* (November 2000).
30. Wiesel, William E. "Perturbations of Relative Satellite Motion about an Oblate Planet.," *Journal of Guidance, Control, and Dynamics* (July 2000).
31. Wiesel, William E. "Relative Satellite Motion about an Oblate Planet," *Journal of Guidance, Control, and Dynamics*, 25(4):776–785 (July-August 2002).
32. Yeh, Hsi-Han and Andrew Sparks. "Geometry and Control of Satellite Formations," *Proceedings of the American Control Conference* (June 2000).

## *Vita*

Matthew Press grew up in a military family where for the majority of his childhood, his father was stationed at SHAPE, Belgium. This gave him the unique opportunity to travel around Europe and develop a passion for sightseeing. After graduating in 1995 from MacArthur High School in San Antonio, Texas, he started his career as a draftsman at US Filter. Yearning for more knowledge and a closer walk with Christ, he enrolled in Oklahoma Christian University. Since then he has had some very interesting jobs including teaching English to natives in Papua New Guinea, assisting with chemical demilitarization at Johnston Atoll, and serving as a missionary in Australia. In the spring of 2001, he graduated with a Mechanical Engineering degree and soon began work as an Egress Engineer for the Air Force. On the 7th of July 2002, he married his high school sweetheart and the love of his life. In August of 2002, he and his wife moved to Dayton, Ohio where he began working on his master's degree at the Air Force Institute of Technology at Wright-Patterson Air Force Base. Before coming to AFIT, he spent his leisure time flying, scuba diving, and grading elementary math exams for his wife. Upon graduation, he plans to enjoy these activities once again.

<b>REPORT DOCUMENTATION PAGE</b>					<i>Form Approved</i> <b>OMB No. 0704-0188</b>	
<small>The public reporting burden for this collection of information is estimated to average 1 hour per response, including the time for reviewing instructions, searching existing data sources, gathering and maintaining the data needed, and completing and reviewing the collection of information. Send comments regarding this burden estimate or any other aspect of this collection of information, including suggestions for reducing this burden to Department of Defense, Washington Headquarters Services, Directorate for Information Operations and Reports (0704-0188), 1215 Jefferson Davis Highway, Suite 1204, Arlington, VA 22202-4302. Respondents should be aware that notwithstanding any other provision of law, no person shall be subject to any penalty for failing to comply with a collection of information if it does not display a currently valid OMB control number. <b>PLEASE DO NOT RETURN YOUR FORM TO THE ABOVE ADDRESS.</b></small>						
<b>1. REPORT DATE (DD-MM-YYYY)</b> 28-03-2004		<b>2. REPORT TYPE</b> Master's Thesis			<b>3. DATES COVERED (From — To)</b> Sep 2002 – Mar 2004	
<b>4. TITLE AND SUBTITLE</b>  GEOMETRIC APPROACH TO ORBITAL FORMATION MISSION DESIGN					<b>5a. CONTRACT NUMBER</b>  <b>5b. GRANT NUMBER</b>  <b>5c. PROGRAM ELEMENT NUMBER</b>  <b>5d. PROJECT NUMBER</b>  <b>5e. TASK NUMBER</b>  <b>5f. WORK UNIT NUMBER</b>	
<b>6. AUTHOR(S)</b>  Press, Matthew J., GS-11, USAF					<b>8. PERFORMING ORGANIZATION REPORT NUMBER</b>  AFIT/GA/ENY/04-M04	
<b>7. PERFORMING ORGANIZATION NAME(S) AND ADDRESS(ES)</b> Air Force Institute of Technology Graduate School of Engineering and Management 2950 Hobson Way, Building 640 WPAFB OH 45433-7765					<b>10. SPONSOR/MONITOR'S ACRONYM(S)</b>  <b>11. SPONSOR/MONITOR'S REPORT NUMBER(S)</b>	
<b>9. SPONSORING / MONITORING AGENCY NAME(S) AND ADDRESS(ES)</b>					<b>12. DISTRIBUTION / AVAILABILITY STATEMENT</b>  APPROVAL FOR PUBLIC RELEASE; DISTRIBUTION IS UNLIMITED.	
<b>13. SUPPLEMENTARY NOTES</b>						
<b>14. ABSTRACT</b>  For distributed remote sensing architectures to be useful for collecting data, it is essential to have a methodology for relating orbital formation parameters to remote sensing requirements. Utilizing the characteristics of formation parameters, an orbital design approach is developed that establishes a satellite formation from a desired instantaneous spatial distribution as viewed from a target ground site. To maintain a conceptually basic representation, a geometric approach is used to develop the correlating algorithm. This tool will enable mission planning for orbital formations as well as future concept exploration.						
<b>15. SUBJECT TERMS</b>  Formation Flying; Stationary Formation; Remote Sensing Distribution; Relative Parameters; Satellite Array; Reconnaissance; Surveillance; Targeting; Satellite Imaging; Mission Analysis; Mission Geometry						
<b>16. SECURITY CLASSIFICATION OF:</b> <b>a. REPORT</b>  U			<b>17. LIMITATION OF ABSTRACT</b>  UU		<b>18. NUMBER OF PAGES</b>  84	
<b>b. ABSTRACT</b>  U			<b>c. THIS PAGE</b>  U		<b>19a. NAME OF RESPONSIBLE PERSON</b> Steven G. Tragesser, PhD, USAF (ENY)	
<b>19b. TELEPHONE NUMBER (include area code)</b> (937) 255-3636, ext 4559						